UNIVERSITY OF CALIFORNIA, SAN DIEGO

Towards a Quantitative Understanding of TNF's Signaling Functions

A dissertation submitted in partial satisfaction of the requirements for the degree of Doctor of Philosophy

in

Chemistry

by

Andrew Bennett Caldwell

Committee in charge:

Professor Alexander Hoffmann, Co-Chair
Professor Daniel Donoghue, Co-Chair
Professor Lars Eckmann
Professor J. Andrew McCammon
Professor Wei Wang

2014

The dissertation of Andrew Bennett Caldwell is approved, and it is acceptable in quality and form for publication on microfilm and electronically:

_____

_____

_____

_____

Co-Chair

_____

Co-Chair

University of California, San Diego

2014

DEDICATION

I would like to dedicate this dissertation to my mother Gwen, my father Marshall, and my brother Grady. I could never have made it here without your constant love, encouragement, and support. Thank you for being there for me every step of the way.

To my grandparents Don and Joyce, who although aren't here to see this completion of this work, throughout my life have provided guidance and love.

And to my fiancé and future wife, Victoria, whose ever constant love and support enabled me to complete this dissertation.

TABLE OF CONTENTS

DEDICATION iv

LIST OF ABBREVIATIONS vii

LIST OF FIGURES ix

ACKNOWLEDGEMENTS xi

VITA xiii

ABSTRACT OF THE DISSERTATION xiv

Chapter 1: General Introduction 1

Inflammation and Innate Immunity 2

Inflammatory Signaling Network 4

Mediatiors of Inflammation 12

Tumor Necrosis Factor 14

Macrophages 21

Systems Biology: Synthesis of Experiment and Simulation 24

Objectives of the Dissertation 27

Chapter 2: Towards a quantitative and modular understanding of TLR-induced TNF production 29

Introduction 30

Materials and Methods 32

Dynamics of TNF production are dependent on kinetics of TRIF and MyD88-mediated signaling events 41

TNF mRNA production is regulated by NFκB, but not IRF 42

A Module for TLR-induced nascent TNF mRNA production 43

TRIF controls TNF mRNA half-life..... 44

A module for TRIF-mediated TNF mRNA stabilization..... 47

TRIF accelerates translation and secretion of TNF mRNA 47

A module for TRIF-mediated promotion of TNF translation and secretion.. 49

Discussion 50

Acknowledgements 54

Chapter 3: Network dynamics determine the autocrine and paracrine functions of TNF 68

Introduction..... 69

Materials and Methods 70

A mathematical model of TLR agonist-responsive TNF production 77

The autocrine signaling function of TNF augments NFκB activation in response to CpG. 78

TLR-agonist induced kinetics of TNF production encodes autocrine and paracrine functions 80

Discussion 82

Acknowledgements 86

Chapter 4: Concluding Discussion and Future Directions 97

REFERENCES 106

LIST OF ABBREVIATIONS

AP-1 - Activated protein 1

BMDMs - Bone Marrow Derived Macrophages

DCs - Dendritic Cells

dsRNA - double stranded RNA

ELISA - Enzyme-linked immuno sorbent assay

EMSA - Electrophoretic Mobiility Shift Assay

FLDMs - Fetal Liver Derived Macrophages

GAPDH - Glyceraldehyde 3-Phosphate Dehydrogenase

IFN - Interferon

IκB - Inhibitor of NFκB

IKK - IκB Kinase

IRAK - Interleukin-1 Receptor-associated Kinase

IRE - Interferon Response Element

IRF - Interferon Regulatory Factor

LPS - Lipopolysaccharide

MyD88 - Myeloid Differentiation Primary-Response Protein-88

NFκB - Nuclear Factor-κB

PAMPs - Pathogen-Associated Molecular Patterns

PBS - Phosphate Buffered Saline

Poly (I:C) - Polyinosine-polycytidylic Acid

PRRs - Pattern-Recognition Receptors

qRT-PCR - Quantitative Real-Time PCR

TBK - Tank-binding kinase

TIR - Toll–interleukin-1 (IL-1) receptor

TLRs - Toll-like receptors

TNF - Tumor necrosis factor

TRIF - Toll–interleukin-1 (IL-1) receptor (TIR) domain–containing adaptor-inducing Interferon-β

TRAF - TNF receptor associated factor

LIST OF FIGURES

Figure 1.1 The Inflammatory and Innate Immune Signaling Network 11

Figure 1.2 Regulation of TNF production 20

Figure 2.1 TRIF and MyD88 Contribute to TNF production 55

Figure 2.2 NFκB is essential for TNF mRNA production 56

Figure 2.3 IRF3 and IRF7 are dispensible for TNF gene transcription and mRNA production 57

Figure 2.4 MyD88 controls early NFκB activation, TRIF controls late activation 58

Figure 2.5 A module for nascent TNF mRNA production 59

Figure 2.6 TRIF controls TNF mRNA stability 60

Figure 2.7 TRIF controls p38, ERK, and MK2 activation 61

Figure 2.8 p38 controls MK2 and TTP phosphorylation 62

Figure 2.9 A module for TRIF-mediated mRNA half-life stabilization 63

Figure 2.10 TRIF have significantly decreased pro-TNF expression 64

Figure 2.11 p38 controls pro-TNF translation 65

Figure 2.12 TRIF controls eIF4E and TACE activation 66

Figure 2.13 A model for TRIF-mediated translation and secretion 67

Figure 3.1 The multi-modular mathematical model for TNF production 87

Figure 3.2 The multi-modular model accounts for LPS-mediated TNF production in wild-type cells 88

Figure 3.3 The multi-modular model accounts for LPS-mediated TNF production in MyD88-deficient cells but not TRIF deficient cells 89

Figure 3.4 The multi-modular model accounts for PolyI:C-mediated TNF production but not CpG-mediated TNF production 90

Figure 3.5 Iterative modification of the multi-modular model leads to TNFR module inclusion 91

Figure 3.6 The multi-modular model with TNF autocrine feedback can predict CpG-induced TNF production 92

Figure 3.7 TLR-responsive TNF production functions in an autocrine manner in response to some TLR ligands but not others. 93

Figure 3.8 Transcriptome analysis reveals autocrine TNF-dependency in certain genes 94

Figure 3.9 CpG-induced autocrine TNF modulates inflammatory gene programs 95

Figure 3.10 LPS-induced TNF signals in a primarily paracrine manner 96

ACKNOWLEDGEMENTS

I would like to acknowledge all of the people that I have worked with in the Hoffmann Lab over the last 6 years. It has been a great experience to work with such a thoughtful, helpful, and kind group of people. I would like to thank my advisor, Alex, for taking me on as a graduate student and guiding me to the completion of this project. I would also like to thank my coworker Brooks Taylor for his helpful profreeding of and feedback concerning this thesis.

Chapter 2, is a modified presentation of material that is being prepared for publication as “Network dynamics determine the autocrine and paracrine signaling functions of TNF” by Caldwell AB, Cheng Z, Vargas A, Birnbaum H, and Hoffmann A. The dissertation author was the primary investigator and author of this material. Zhang Cheng performed the mathematical modeling and computational simulations. Christine Cheng provided RNA from LPS-stimulated FLDMs for mature mRNA analysis.

Chapter 3, is a modified presentation of material that is being prepared for publication as “Network dynamics determine the autocrine and paracrine signaling functions of TNF” by Caldwell AB, Cheng Z, Vargas J, Birnbaum H, and Hoffmann A. The dissertation author was the primary investigator and author of this material. Zhang Cheng performed the mathematical modeling and computational simulations. Jesse Vargas performed immunofluorescence microscopy imaging and analysis of immunofluorescence data. Harry

Birnbaum performed the analysis of the transcriptome data. Kim Ngo provided assistance with the creation of cDNA libraries for RNA sequencing.

VITA

Education

2008-2014	University of California San Diego, San Diego, CA Doctor of Philosophy in Chemistry
2008-2010	University of California San Diego, San Diego, CA Master of Science in Chemistry
2004-2008	Seattle Pacific University, Seattle, WA Bachelor of Science in Chemistry, Bachelor of Science in Biochemistry, Cum Laude

Fellowships

2009-2011	Molecular Biophysics Training Grant

ABSTRACT OF THE DISSERTATION

Towards a Quantative Understanding of TNF's Signaling Functions

by

Andrew Bennett Caldwell

Doctor of Philosophy in Chemistry

University of California, San Diego, 2014

Professor Alexander Hoffmann, Co-Chair

Professor Dan Donoghue, Co-Chair

A critical aspect of the macrophage inflammatory response to pathogen challenge is the rapid production of TNF that signals in autocrine and

paracrine manners to carry out innate and adaptive immune responses. Toll-Like Receptors (TLRs) are highly expressed in macrophages, and recognize extracellular and intracellular pathogen signals leading to the activation of transcription factors and cytokine production. There have been numerous TLR-mediated signaling mechanisms identified that control the production of TNF, but it remains unclear how they coordinate together in macrophages.

This dissertation details a systems biology approach to develop a quantitative understanding of how TNF is produced and signals in the context of the macrophage inflammatory signaling network. Chapter 1 presents an overview of the inflammatory and innate immune signaling network that coordinates the production of TNF in macrophages, as well as a description of the field of computational systems biology. Chapter 2 describes the quantitative, experimental characterization of modules for each step in TNF production: gene transcription, mRNA half-life stabilization, translation, and secretion. Mathematical models are designed from the module architechure that can recapitulate experimental data, and the three simple models are linked to provide a model for TNF production. In Chapter 3, the TNF production model is connected to previously described TLR, TNFR, and NFκB signaling modules to create a multi-modular model for TNF production and signaling in the context of the inflammatory signaling network. Unexpectedly, the model predicts and it is subsequently experimentally confirmed that CpG-induced TNF signals in an autocrine manner to prolong NFκB activation and

modulate gene expression programs. In contrast, lipopolysaccharide signals in a primarily paracrine manner.

Lastly, Chapter 4 provides a discussion on the unique modular approach to systems biology presented in this thesis, the stimulus-specific encoding of autocrine and paracrine TNF signaling functions, and comments on the ways the multi-modular model can be used to make new predictions as well as a potential direction for future work on the iterative expansion of the model to further describe the inflammatory and innate immune signaling network.

Chapter 1: General Introduction

Inflammation and Innate Immunity

Surveillance, recognition, and response to pathogens are vital processes undertaken by host organisms to ensure overall health. These processes, along with response to tissue damage, constitute the innate immune system (Takeuchi and Akira, 2010). Many different types of host cells are able to sense and recognize pathogens, but the classical examples of innate immune cells are natural killer cells (NKs), dendritic cells (DCs), and macrophages (Kawai and Akira, 2006). These immune cells specialize in sensing components of microorganisms, such as viruses, bacteria, and fungi, through a variety of pattern recognition receptors (PPRs) highly expressed in either the membrane or the cytoplasm. PPRs recognize a variety of structures, both microorganism-specific and highly conserved, known as pathogen-associated molecular patterns (PAMPs). The Toll-like receptor (TLR) family is the most well known family of PPRs, which respond to various PAMPs by eliciting signaling events within the innate immune signaling network. This leads to the production of cytokines and chemokines, which are intracellular signaling molecules that coordinate diverse inflammatory and immune responses that aid in the clearance of the infecting pathogen. The acute production of cytokines by these innate immune cell types, inducing the removal of microbial infection, constitutes the process known as inflammation.

These signaling processes are predominantly transient, occurring on a timescale of minutes to hours, and are classically considered as the first line of

defense against a pathogen infection. While the adaptive immune system, which consists predominately of B and T lymphocytes that carry humoral and cell-mediated immune processes that occur on a much longer timescale, has traditionally thought to be only part of the immune system that is pathogen-specific, there is considerable pathogen-specificity encoded both within the diversity of agonists recognized by PPRs and the innate immune signaling network dynamics brought about by PPR activation (Iwasaki and Medzhitov, 2010; Kawai and Akira, 2010). Furthermore, the pathogen-specific recognition and response carried out by the innate immune system is essential for modulating the adaptive immune response; DCs and macrophages both play a large role in priming and activating adaptive immune B and T cells through their antigen presentation, cytokine, and chemokine production (Hoebe et al., 2004; Iwasaki and Medzhitov, 2010).

Therefore, the production of pro-inflammatory cytokines is essential not only in the acute phase response, but in the adaptive response as well. Consequently, the dynamics of cytokine production are tightly regulated, as aberrant or uncontrolled cytokine production can lead to a variety of disease states (Takeuchi and Akira, 2010). Understanding how the dynamics of cytokine production are controlled in a pathogen-specific manner informs the role that a cytokine plays in inflammation and the innate immune response, as well as the effect it has on modulating adaptive. This thesis will focus on the pathogen-specific control of one essential cytokine, tumor necrosis factor

(TNF), and the paracrine and autocrine signaling dynamics brought about by TNF production in the context of the macrophage pathogen response.

Inflammatory Signaling Network

Innate immune cells sense chemical structures and patterns associated with various pathogens through PRRs located on the plasma membrane and endosome, leading to the activation of kinases and transcription factors. These signal transducers upregulate the production of cytokines, chemokines, and interferons that lead to the clearance of pathogens, attenuation of inflammation, and modulation of adaptive immunity. The production of these mediators of inflammation is a complex and highly regulated process, carried out through an inflammatory signaling network that encodes pathogen specificity through the types of receptors and the network dynamics that the receptor-associated proteins elicit. The dynamics of cytokine production, therefore, must be understood within the context of the receptors, adaptors, kinases, and transcription factors that make up the inflammatory signaling network.

Four main types of PRRs have been identified: the aforementioned TLRs and the C-type lechtin receptors (CLRs), both located within the membrane; and the NOD-like receptors (NLRs) and Retinoic acid-inducible gene (RIG)-I-like receptors (RLRs), located in the cytoplasm. Of the PRRs, the most well-studied family of receptors are the TLRs (Kawai and Akira, 2010; Takeuchi and Akira, 2010). The gene *toll* was first identified in 1994 to have a

key role in the *Drosophila melanogaster* immune response to fungal infection, and the subsequent discovery of human receptors with homology to *toll* led to their current designation. Furthermore, it was determined that the previously identified interluekin-1 receptor (IL-1R) shared a similar cytoplasmic domain with both *toll* and the human TLRs. To date, there have been 10 TLRs identified in humans (TLRs 1-10) and 12 in mice (TLRs 1-9;11-13) (Takeuchi and Akira, 2010). The TLRs consist of leucine-rich repeats (LRRs) at the N-terminus, a transmembrane domain, and a Toll/IL-R homology (TIR) domain located in the cytoplasm. They recognize a variety of molecular structures associated with pathogens, such as lipopolysachharide, flagellin, bacterial DNA, and viral RNA through their LRRs. Upon engagement of the surface LRRs, the receptors recruit TIR domain-containing adaptors such as MyD88, TIRAP (Mal), TRIF, and TRAM through their own TIR-domain. MyD88 is exclusively associated with all TLRs with the exception of TLR3, which signals through TRIF, and TLR4, which signals through both MyD88 and TRIF. The adaptor TIRAP is involved in recruiting MyD88 to TLR2 and TLR4, while TRAM is involved in recruiting TRIF to TLR4. TLRs are found expressed on either the cell surface or intracellular vesicles such as endosomes, lysosomes, or the endoplasmic reticulum (ER). The cell surface receptors consist of TLR1, TLR2, TLR4, TLR5, TLR6, and TLR11 and primarily sense components of bacteria; in contrast, TLR3, TLR7, TLR8, and TLR9 are mainly endosomal-located, and sense viral or bacterial-associated nucleic acids.

Uniquely, the receptor that senses bacterial LPS, TLR4, signals through both the adaptors MyD88 and TRIF. Upon receptor engagement, TIRAP recruits MyD88 to the receptor, leading to subsequent MyD88-mediated kinase and transcripton factor activation. Following these MyD88 signaling events, the engaged TLR4 receptor is trafficked to endosome, where it can recruit TRIF through TRAM to lead to TRIF-mediated kinase and transcription factor activation.

The adaptors MyD88 and TRIF engender cytokine production through the coordinated activation of downstream kinases and transcription factors. Once recruited to the receptor, MyD88 recruits three kinases that activate sequentially through phosphorylation: IRAK4, IRAK1, and IRAK2 (Kawai and Akira 2010). The activation and localization to the receptor of these IRAKs allows them to recruit the E3 ligase TRAF6, which conjugates polyubiquitin chains linked through Lys63 of ubiquitin (K63-linked chains) onto IRAK1 and itself. These K63-linked chains, constructed in conjunction with the E2 ligase Uev1A and Ubc13, form scaffolds that recruit and activate the TAK1 kinase complex through its interaction with ubiquitin-binding domain containing TAB2 and TAB3 (Akira et al., 2006; Kawai and Akira, 2010; Shih et al., 2011; Takeuchi and Akira, 2010). Furthermore, the NFκB kinase complex IKK, consisting of IKKα, IKKβ, and the ubiquitin-binding NEMO, is recruited to these scaffolds in close proximity to the TAK1 complex, whereby IKKβ can be phosphorylated and activated by TAK1. In addition to activating the IKK

complex, TAK1 is responsible for the activation of a large subset of mitogen-activated protein kinases (MAPKs), including ERK1/2, p38, and Jnk kinases through phosphorylation (Kawai and Akira, 2010; Shih et al., 2011; Takeuchi and Akira, 2010). The activation of these MAPKs leads to activation of transcription factors like AP-1, but are also essential for the post-transcriptional control of cytokine production (Clark et al., 2009).

While MyD88 mediates the activation of the transcription factor NFκB (and to a lesser extent, AP-1), TRIF mediates the activation of NFκB as well as the transcription factor IRF3. However, TRIF-mediated kinase activation differs from MyD88; while TAK1 activation is brought about by an analogous pathway as MyD88, TRIF also leads to TAK1 activation through the recruitment of TRADD, which binds the TAK1-activation kinase RIP1 and induces its activation through the recruitment of the E3 ligase Pellino-1. Furthermore, the TRIF-dependent pathway also leads to the activation of two non-canonical IKKs, IKKε and TBK1. The activation of these two kinases is brought about by TRAF3, which TRIF recruits to receptor on the endosome. IKKε and TBK1 then act to phosphorylate IRF3, leading to its dimerization and translocation to the nucleus. Once there, IRF3 is able to bind interferon response elements (IREs) and activate transcription of type-one interferons (IFN-I) and other innate immune response genes (Kumar et al., 2011; Takeuchi and Akira, 2010).

In resting cells, the transcription factor NFκB is located within the cytoplasm, existing as a dimer bound to its inhibitor, IκB. Upon pathogen recognition, signaling events lead to the activation of the kinase for IκB, IKK. When activated, IKK phosphorylates IκB at Ser^{32} and Ser^{36} in the N-terminus, which recruits the E3 ligase βTRCP. βTRCP subsequently conjugates K48-linked ubiquitin chains onto IκB, which designates it for degradation through the 26S proteasome (Shih et al., 2011). Once no longer bound to IκB, NFκB is able to translocate to the nucleus and initiate transcription of genes with κB-site-containing promoters.

The NFκB signaling system plays a critical role in the regulation of inflammation, innate immunity, and development. As a result, misregulation of NFκB activity can lead to numerous autoimmune, chronic inflammatory, and cancer disease states (Karin 2006). The NFκB family of transcription factors consists of five members: *rela* (p65), *relb* (RelB), *crel* (cRel), *NFκB1* (p50/p105), and *NFκB2* (p52/p100). These proteins exist as both homo- and heterodimers, able to bind DNA and dimerize through their common Rel homology domain (RHD). However, not all protein complexes are able to function as a transcriptional activator; p50 and p52 do not contain a transcriptional activation domain (TAD). While there are 15 possible homo- and heterodimer complexes, only 9 are able to activate transcription. Further, while the homo- and heterodimers consisting of p50 and p52 are able to bind DNA, three RelB-containing dimers are not known to bind DNA. In the context

of signaling downstream of TLRs and pro-inflammatory cytokine receptors, the best-studied NFκB dimer is RelA:p50 (O'Dea and Hoffmann, 2009, 2010).

The inflammatory signaling network involves multiple branches of pathways emanating from a diverse set of PRRs, with each branch having unique temporal kinetics. However, these signaling branchs eventually lead back to a common set of transcription factors. The combination of differential pattern recognition by specific TLRs and the temporal separation of signal transduction by different branches of the signaling network encode pathogen-specific temporal dynamics of transcription factor activation. For example, whereas TLR4 utilizes both MyD88 and TRIF, there is a temporal separation between their respective activation of NFκB. MyD88-mediated dynamics are earlier but more transient, as TLR4 is quickly trafficked away from the plasma membrane to the endosome; in contrast, TRIF-mediate dynamics have slower onset but longer persistence, as TRIF is not recruited until the engaged TLR4 receptor has been trafficked to the endosome. Furthermore, the dynamics of NFκB attenuation are stimulus-specific as well; once of the first genes activated by NFκB is IκBα, leading to the fast production IκBα protein which can bind NFκB and sequester it back into the cytoplasm. In the context of signaling downstream of TNF activation, NFκB rapidly transcriptionally activates the gene *a20*, a zinc-finger protein that modifies ubiqutin scaffolds upstream of IKK leading to downregulation of NFκB activity (O'Dea and Hoffmann, 2009, 2010; Takeuchi and Akira, 2010).

In summary, the inflammatory signaling network contains a diverse set of pathogen-sensing receptors leading to pathways that activate transcription factors and subsequently induce the production of pro-inflammatory cytokines, mediating inflammation. The complexity of the signaling network at the levels of receptors, adaptors, kinases, and transcription factors allows for pathogen-specific responses to be encoded within the temporal dynamics of NFκB activation and cytokine production (O'Dea and Hoffmann, 2009, 2010).

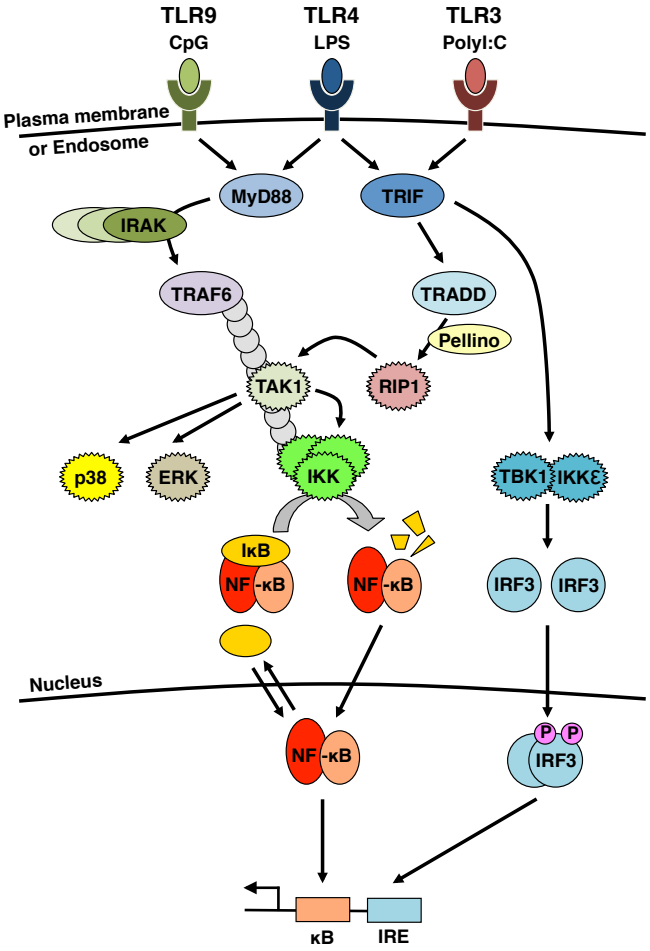

Figure 1.1 The Inflammatory and Innate Immune Signaling Network
Activation of TLRs by pathogen signals leads to the recruitment of the adaptors MyD88 and TRIF. These adaptors recruit kinases, which through various kinase pathways bring about the activation of the IKK complex and TBK1/IKKε. IKK mediates the degradation of IkB, allowing NFκB to translocate to the nucleus and effect gene transcription. TBK1/IKKε phosphorylate the transcription factor IRF3, leading to its dimerization and translocation to the nucleus.

Mediatiors of Inflammation

Inflammation is a complex innate immunity program that brings about pathogen clearance, wound healing, and tissue remodeling. The inflammatory response involves the coordination of a variety immune cell types sensing the initial pathogen signal and secreting factors that recruit other cell types to sites of infection and damage. These secreted factors that propagate and mediate inflammation include pro-inflammatory and anti-inflammatory cytokines, interferons, chemokines, nitric oxide, prostaglandins and histamines. Pro-inflammatory cytokines such as IL-1 and TNF are rapidly produced upon pathogen challenge, and further mediate inflammation through activation of transcription factors, chiefly NFκB.

Members of the interleukin family signal through receptors that share some homology with the TLRs, and elicit activation of pathways within the inflammatory signaling network similar to PAMPs. Interluekins like IL-1, IL-6, and IL-12 are involved in acute phase inflammation, hematopoiesis through growth factor production, and T and B cell recruitment and proliferation through chemokines. TNF rapidlyactivates NFκB with similar dynamics to IL-1, however the receptors and adaptors used to bring about IKK activation differ. In addition to inducing strong pro-inflammatory cytokine and chemokine in the acute phase response, TNF is involved in promoting cell proliferation, recruiting and modulating T and B cells, regulating phagocytosis, and granuloma formation.

In contrast, the Type I family of interferons (IFNα and IFNβ) are primarily involved in upregulating host defense mechanisms through the activation of DCs, activation of T-cells and Th1 polarization, the production of chemokines to recruit leukocytes, and the upregulation of a particular subset of innate immune genes know as interferon-stimulated genes (ISGs) (Nakaya et al., 2001). Interferons were originally named for their involvement in interfering with viral replication, and play a key anti-viral and immunomodulatory role (Pestka et al., 2004; Platanias, 2005; Striz et al., 2014).

Chemokines serve as another essential type of mediator of the inflammatory process. These small proteins are secreted by a variety of cells, and their primary role is the recruitment of diverse immune cell types to sites of inflammation and tissue damage through chemotaxis. While chemokines serve as a strong link to adaptive immunity through their near universal recruitment of T cells to wound sites, many also play a significant role in inflammation through the recruitment and modulation of innate immune cells, angiogenesis, and hematopoiesis (Charo and Ransohoff, 2006; Damme and Mantovani, 2005; Striz et al., 2014).

Pro-inflammatory cytokines, interferons, and chemokines all play essential roles in the acute response to pathogens, propagation of inflammation, recruitment of specialized immune cells, attenuation of inflammation, and modulation of the adaptive immune program. However, after

upregulating the genes needed for bacterial clearance and inflammatory resolution the initial first wave of pro-inflammatory cytokine production must be attenuated so as not to lead to chronic inflammation and disease states. Therefore, a comprehensive understanding of the tight regulation of acute phase pro-inflammatory cytokine production and signaling functions is particularly relevant to further characterizing the role that cytokines like TNF carry out in innate and adaptive immunity.

Tumor Necrosis Factor

Pro-inflammatory cytokines carry out diverse functions, with a considerable ability to modulate not only inflammation, but also the innate and adaptive immune responses as a whole. Tight temporal regulation of production by host cells is essential to properly remove infecting pathogens as well as prevent disease states that can arise from chronic inflammation. Of all the cytokines involved in inflammation and immunity, perhaps the most ubiquitous in its production and diverse in its function is TNF. In addition to its well-known role of propagating the initial signal of pathogen challenge and being a master regulator of pro-inflammatory cytokine production, TNF also plays a role in cell death and proliferation, differentiation, migration, phagocytosis, and survival. However, aberrant TNF production can lead to a variety of disease states, including cancer, diabetes, atherosclerosis, and autoimmune disorders such as inflammatory bowel disease and rheumatoid

arthritis (Parameswaran and Patial, 2010; Waters et al., 2013). Furthermore, the connection between bacterial infection and autoimmune disorders resulting from TNF misregulation is well reported. Therefore, a mechanistic and quantatitive understanding of the production and subsequent role in inflammatory signaling of TNF is of particular importance.

The history of the discovery of TNF begins with work in the early 1960s published by O'Malley *et al.* that demonstrated that the tumor necroptotic ability of bacterial endotoxin was indirect, and that there existed a factor produced within serum of LPS challenged animals that conferred this tumor killing functionality (O'Malley et al., 1962). This factor was identified in 1975, and termed 'tumor necrosis factor', which was later isolated and cloned (Aggarwal et al., 1985; Carswell et al., 1975; Shirai et al., 1985; Wang et al., 1985). Concurrent with the discovery and characterization of tumor necrosis factor was the study of wasting, or cachexia. It was determined that a factor produced by macrophages in response to bacterial infection could lead to formation of the disease state associated with cachexia, and this factor was termed cachectin (Beutler et al., 1985b, 1985b; Kawakami and Cerami, 1981). It was soon discovered that tumor necrosis factor and cachectin were in fact the same protein, an early demonstration of the breadth of TNF function (Beutler et al., 1985a).

The factor that came to be known as TNF was first discovered as a protein secreted by macrophages, but its production is not limited to that cell

lineage; a variety of immune cell types, including DCs, neutrophils, NKs, and T cells, can produce and secrete TNF (Akira et al., 1990; Grivennikov et al., 2005; Serbina et al., 2003). The production of TNF is elicited by numerous PAMPs and pro-inflammatory cytokines, including IL-1 and TNF (Bethea et al., 1992; Werner et al., 2005). NFκB and IRF3, transcription factors downstream of TLRs and their adaptors MyD88 and TRIF, have been previously implicated in controlling TNF transcription (Covert et al., 2005; Drouet et al., 1991; Lee et al., 2009; Wesche et al., 1997; Yamamoto et al., 2003; Zhao et al., 2008). Gene transcription is not the only level of control of TNF production, however: TNF has been shown to be regulated post-transcriptionally through the control of its mRNA half-life, protein translation, and secretion (Andersson and Sundler, 2006; Black et al., 1997; Han et al., 1991a, 1991b). Because of this, the temporal kinetics of TNF secretion by cells responding to stimuli depend on multiple steps of production control, which may be modulated differentially depending on stimuli.

As highlighted previously, TLR agonists such as LPS activate multiple kinase and transcription factor pathways. In the case of TNF production, MAPK pathway activation has been shown to control various steps in the maturation of TNF from nascently transcribed mRNA to secreted protein. The 3’ untranslated region of TNF mRNA contains a series of palindromic AU sequences, termed AU-repeat elements (AREs), which are recognized by multiple types of proteins for binding (Han et al., 1991a, 1991b). These

proteins, such as TTP or HuR, have been shown to either designated the TNF mRNA for degradation or prolong its existence, respectively (Carballo et al., 1998; Fan and Steitz, 1998; Kontoyiannis et al., 1999; Lai et al., 1999; Peng et al., 1998). Unphosphorylated TTP can bind ARE-elements in mRNA and localize the mRNA to processing bodies (p-bodies), small compartments in the cytoplasm which contain machinery for degrading mRNA (Sandler and Stoecklin, 2008). In unstimulated cells, this process occurs constitutively, causing TNF to have a half-life as short as 7 minutes (Hao and Baltimore, 2009). However, a MAPK known as MK-2 which downstream of canonical MAPKs ERK1/2 and p38, has been shown to phosphorylate TTP on Ser^{52} and Ser^{178}, which allows TTP to be bound by the protein complex 14-3-3 which decreases the ability of TTP to direct the degradation of TNF mRNA (Hitti et al., 2006; Johnson et al., 2002; Kotlyarov et al., 1999; Ronkina et al., 2007; Stoecklin et al., 2004). This leads to an increase in half-life of TNF mRNA as much as six-fold, stabilizing TNF message and allowing more mRNA to be translated into protein (Hao and Baltimore, 2009).

In addition to half-life stabilization, there have also been mechanisms reported on the promotion of translation of TNF mRNA. The MAPK Mnk-1 and its target eukaryotic initiation factor 4E (eIF4E), a protein that likely recruits mRNAs to translational machinery, have been implicated in the control of TNF mRNA translation (Andersson and Sundler, 2006; Topisirovic et al., 2004; Wang et al., 1998). Furthermore, it has been reported that the MAPK MK-2,

shown to stabilize mRNA messages, may also control or promote the translation of TNF mRNA (Gais et al., 2010).

TNF is translated as 27kDa pro form of the protein, known as mTNF or pro-TNF. This form contains a membrane-spanning domain that anchors the protein to the plasma membrane. In order to be secreted, proTNF is proteolytically cleaved by a metalloprotease called TNF converting enzyme (TACE), which converts the protein into a 17kDa molecule that forms a homotrimer in its biologically active form (Black et al., 1997; Parameswaran and Patial, 2010; Smith and Baglioni, 1987). TACE functions downstream of the MAPKs p38 and ERK1/2, which phosphorylate and activate the enzyme on Thr^{735} (Díaz-Rodríguez et al., 2002; Fan and Derynck, 1999; Soond et al., 2005; Xu and Derynck, 2010). These studies highlight the fact that TNF production is highly regulated in response to stimuli, shaping the kinetics of TNF secretion through the activation of multiple pathways used by stimulus-sensing receptors.

There has been considerable research on the diverse ways that TNF propagates inflammatory signals through paracrine signaling, the signaling process whereby TNF is secreted by a responding cell, and then sginals to neighboring cells of similar or dissimilar lineage. This paracrine signaling effect of TNF is essential for its activity to recruit diverse cell types and modulate the inflammatory and immune response. However, TNF can also signal in an autocrine manner, where the cell that responds to a stimuli and secretes TNF

can also sense the TNF it has just produced; this phenomenon has been documented as an essential aspect of TLR-induced inflammatory signaling (Blasi et al., 1994; Coward et al., 2002; Kuno et al., 2005; Lombardo et al., 2007; Wu et al., 1993; Xaus et al., 2000). Indeed, the balance between autocrine and paracrine signaling functions of TNF was proposed early on in the study of intracellular bacteria infections as an important feature of pathogen response, as well as in mounting a response that addresses infection without developing autoimmune disorders (Kindler et al., 1989; Zhan et al., 1996). Furthermore, recent studies have reported that mice with a bioactive transmembrane-bound TNF which is unable to be secreted are still able survive physiological doses of the intracellular bacteria *L. monocytogenes*, though paracrine TNF signaling is abrogated (Alexopoulou et al., 2006).

The cytokine TNF is expressed and secreted by a variety of immune cells and non-immune cells responding to pathogen challenge or pro-inflammatory paracrine cytokine signaling, and itself controls not only pro-inflammatory cytokine production, but many essential cellular functions including cell death and proliferation, differentiation, migration, phagocytosis, and survival. The regulation of kinetics of TNF production and release are particular importance, as aberrant production can lead to variety of autoimmune disorders and diseases.

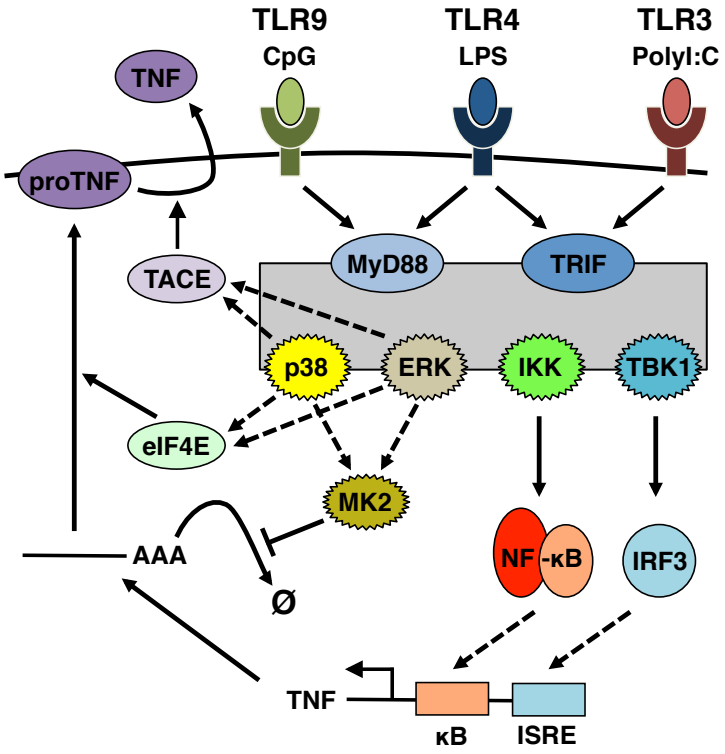

Figure 1.2 Regulation of TNF production
Diagram illustrating mechanisms potentially regulating the production of TNF; solid lines indicate known mechanisms, dashed lines indicate mechanism that have been reported in the literature in differing cell systems. TLR agonists such as LPS, CpG, or PolyI:C engage their respective TLRs, leading to the recruitment of adaptors MyD88 and TRIF. These adaptors lead to the activation of transcription factors NFκB and IRF3, which have been implicated in TNF gene transcription. TNF is also modulated at the level of mRNA stability, translation and secretion, but the mechanisms and adaptor control are not clear.

Macrophages

Macrophages are a myeloid-lineage cell type that have remarkable plasticity in their function and response in the context of innate and adaptive immunity. Traditionally, macrophages have been classified as either pro-inflammatory and classically activated, designated as M1 lineage, or wound-healing and alternatively activated, designated as M2 lineage. However, recent advances in the field on the diverse functions that macrophages carry out suggest that the paradigm of macrophages existing on either of the extreme M1 or M2 is no longer appropriate. Rather, there is a spectrum of types of macrophages, that can carry out many types of functions including responding to pathogens and eliciting inflammation, wound-healing/tissue remodling, and regulating innate and adaptive immunity (Mosser and Edwards, 2008). The roles that a particular macrophage can play are very dependent on the context of where it is localized; furthermore, macrophages have considerable ability to switch between roles, given the proper intercellular and extracellular contextual signals. While M1 macrophages are primarily known for the pro-inflammatory cytokine production and phagocytic activity, the proper modulation of the macrophage response both by other immune cells as well as by macrophages themselves is essential for the propagation of an initial stress or pathogen and the subsequent resolution of inflammation.

In the context of responding to pathogen and infection and inflammatory signaling, however, macrophages serve as sentinels of the

innate immune system (Murray and Wynn, 2011). Macrophages begin as myeloid progenitor cells in the bone marrow, where they are directed down a lineage line from monoblasts, to pro-monocytes, and then monocytes. At this stage, they are released and targeted to circulate in the blood stream. From here, monocytes are able to transport from the blood stream into various tissues, where they are directed through signaling from their tissue environment towards a finalstage of maturation, such as alveolar macrophages (lung), Kupffer cells (liver), and osteoclasts (bone) (Mosser and Edwards, 2008; Murray and Wynn, 2011). In order to reach a M1 state of classical activation, tissue-resident macrophages must be stimulated by the combination of two stimuli: IFNγ and TNF. The signaling conjunction of these two cytokines, traditionally secreted by T_H1 and NK cells, enhances the macrophage capacity to produce pro-inflammatory cytokines and carry out host defense against microorganisms. However, TNF and another IFN family member IFNβ are produced by macrophages responding to LPS, through the activation of the TLR4 adaptors MyD88 and TRIF leading to NFκB and IRF3 activation. The IFNβ produced by macrophages is able to replace the requisite IFNγ needed for M1-like lineage determination, and thus when sensing pathogens, macrophages are able self-activate and modulate towards a M1 state (Mosser and Edwards, 2008).

Classically activated tissue resident macrophages are often the first line of defense of host innate immunity, and rapid and strong pro-inflammatory

cytokine production is a hallmark mechanism by which they carry out pathogen clearance. Of all the pro-inflammatory cytokines that macrophages produce, TNF is perhaps the most essential to macrophage function. Macrophages produce high levels of TNF in response to PRRs and cytokines such as IL-1 and TNF. The signaling effect of secreted TNF is important for macrophage inflammatory function, including regulation of iNOS production, phagocytic activity, and inflammatory resolution (Aderem and Underhill, 1999; Michlewska et al., 2009; Salkowski et al., 1997).

In summary, classically activated macrophages play a key role in the initial response to pathogen infection, propagation of inflammatory signal, clearance of infection, and resolution of inflammation. They carry out these functions largely in part through the production of pro-inflammatory cytokines, chiefly TNF, which serves to recruit specified cell types to sites of infection through induction of gene programs for chemokine production and attenuation of inflammation. The tight regulation of TNF production in macrophages, therefore, is essential for the proper response to pathogens and subsequent downregulation, as many of the TNF-associated disease states have been demonstrated to be largely caused by macrophage misregulation (Biswas and Mantovani, 2010; Gillett et al., 2010; Waters et al., 2013).

Systems Biology: Synthesis of Experiment and Simulation

The field of computational systems biology has aggressively pursued the synthesis of experiment and simulation in developing mathematical models that are able to make quantitative predictions of the complex dynamics and outcomes of large signaling networks. While many individual signaling pathways have been studied in-depth, particularly systems related to inflammation and innate immunity, there still exists a deficiency in the understanding of how signaling networks act on a global scale.

In order to develop a deeper quantitative prediction of network dynamics, there have been two main approaches within the field: a data-driven modeling approach, and a physicochemical modeling approach. In the first approach, large data sets of biochemical readouts are produced in a model cell type in response to set of perturbations, and the relationship between perturbations (inputs) and biochemical measurements (outputs) are determined by statistical regression methods. These data sets often include the measurements of mRNA induction, protein production, and protein secretion in measurement numbers approaching tens of thousands (Janes et al., 2005, 2006). This data-driven modeling approach has shown considerable predictive ability with regards to determining the end signaling result due to a particular stimulus (Feldman et al., 2013; Janes et al., 2005, 2006). However, there are drawbacks to this approach; the statistical methods used to infer pathway relationships have difficulty in predicting mechanisms of interaction.

Furthermore, the predictive ability of this data-driven approach is often confined to the particular set of perturbations or cell system used to train the computational model. As a result, the predictions made by the computational model often don't translate well to other analogous systems or networks.

The second common approach taken is physicochemical modeling, which uses physical information from the characterization of protein-protein interactions and mass-action, enzyme kinetics to create mathematical models (Aldridge et al., 2006). While these models are often able to recapitulate experimental data of small interaction networks, the fine-grained experimental data needed means that this approach is difficult to scale up to large signaling networks. Furthermore, there is considerable difficulty concerning the parameterization of physicochemical models so that they can make meaningful predictions of the signaling networks they describe.

A recent approach that blends these two methods has come to be known as modular biology (Hartwell et al., 1999; Kitano, 2002; Mallavarapu et al., 2009a). In this approach, signaling networks are broken down into discrete modules, units of signaling interactions with minimal inputs and outputs. Here, the topology of the module is similar to the physicochemical approach, with simple molecular interactions making up each module. However, like the data-drive approach, the dynamics of explicit inputs and outputs are measured at a quantitative level. While the parameters within each module are not based on measured rate reactions, the biochemical data acquired from proteins within

the module, as well as from inputs and outputs of the model, is used to parameterize the mathematical model based on each module. A major strength of this approach is that the modules are interchangeable and complex signaling networks can be built by combining building-block modules.

Previously, our lab has identified modules within the NFκB pathway and blended experiment and simulation to make mathematical models describing IKK signaling to NFκB and TNFR signaling to IKK (Hoffmann et al., 2002; Werner et al., 2005, 2008). In the chapter 2 of this thesis project, we use the modular approach to experimentally and computationally characterize each step in the regulation and production of TNF in TLR-induced macrophage inflammatory signaling. As the production and secretion of TNF is dynamic process, with both paracrine and autocrine signaling, a quantitative understanding of how TNF signals within the TLR-NFκB-TNF signaling network is still needed. Therefore, chapter 3 of this thesis project focuses on building a multi-modular model for the TLR-NFκB-TNF signaling network, combining the previously published modules for TLR signaling to IKK, TNFR signaling to IKK, and IKK signaling to NFκB with the TNF production model presented in chapter 2 to make predictions about the stimulus-specific autocrine and paracrine signaling functions of TNF.

Objectives of the Dissertation

Macrophages are considered as sentinels of the immune system; they are often the first responders to pathogen challenge and elicit the propagation of inflammation through the production of cytokines. TNF is an essential cytokine rapidly secreted by macrophages in response to pathogen infection and signals to diverse immune cell types with pleitropic functions.

The introduction provided an overview of the inflammatory and innate immune signaling network in the context of TLR-induced signaling. There have been many mechanisms reported for the regulation of TNF production in this signaling network, but given the diverse cell systems used, it is not clear which are relevant for macrophages, nor which adaptors control those mechanisms. Chapter 2 of the dissertation will center on quantifying discrete steps in the production of TNF, determining the mechanisms that control TNF processing, and constructing simple mathematical models to describe these complex events.

A modular, systems biology approach to signaling networks has been previously used to achieve considerable qualitative and quantitative insights. In chapter 3 of the dissertation, the mathematical models for each step in TNF production will be linked together and connected to modules for TLR, TNFR, and NFκB to construct a multi-modular model for TNF production and signaling in the context of the inflammatory response to pathogens. This model will then be simulated to make predictions about the stimulus-specific

autocrine and paracrine functions of TNF, which will subsequently be experimentally verified and explored further.

Chapter 2: Towards a quantitative and modular understanding of TLR-induced TNF production

Introduction

Tumor necrosis factor (TNF) is a key inflammatory cytokine produced by macrophages exposed to pathogens. The Toll-Like Receptor (TLR) family of receptors recognizes a variety of molecular substances derived from pathogens such as bacteria, viruses, and fungi, eliciting signaling events that coordinate inflammatory and innate immune responses (Kawai and Akira, 2010). TLRs are expressed in many cell types, but perhaps one of the most relevant types for the innate immune response are those of classically activated (M1) macrophages. A hallmark of M1 macrophages and a primary role that they carry out in the innate immune response is the production of pro-inflammatory cytokines, including the ubiquitously expressed TNF (Mosser and Edwards, 2008; Parameswaran and Patial, 2010). In macrophages, TLRs utilize two adaptors which mediate the signaling events leading to pro-inflammatory cytokine production: TRIF and MyD88 (Häcker et al., 2000; Hoebe et al., 2003; Kawai et al., 1999; Sato et al., 2003; Yamamoto et al., 2003). While all TLRs with the exception of TLR3 use the adaptor MyD88, TLR4 uniquely uses both MyD88 and TRIF, which signal from the cell membrane and endosome, respectively (Kawai and Akira, 2010). These adaptors mediate the activation of transcription factors such as NFκB and IRF3, both of which have been implicated in the control of TNF production (Covert et al., 2005; Drouet et al., 1991; Lee et al., 2009; Wesche et al., 1997; Yamamoto et al., 2003).

The production of TNF is not only regulated at the level of gene transcription, but post-trascriptionally through mRNA half-life stabilization, protein translation, and protein secretion (Andersson and Sundler, 2006; Black et al., 1997; Han et al., 1991a, 1991b). Previous reports have sought to determine whether the adaptors TRIF or MyD88 are responsible for these post-transcriptional production control mechanisms, but the conclusions have been mixed; while some reports have argued that TRIF is essential for TNF mRNA half-life control, others have suggested that TRIF is dispensable, or that MyD88 is in fact necessary (Datta et al., 2004; Gais et al., 2010; Hitti et al., 2006; Ronkina et al., 2007; Wang et al., 2011). Given the different conclusions that have been made in various cellular systems with respect to which adaptor controls each of these post-transcriptional processes, we sought to characterize the TRIF and MyD88-mediated mechanisms of TNF production control in primary macrophages.

A fruitful trend in signaling biology has been the approach of combining experiment studies with mathematical models to achieve quantitative and qualitative insights that would not be possible with either alone, an approach that our lab has used extensively (Kearns et al., 2006; O'Dea et al., 2007; Werner et al., 2005, 2008). By constructing simple models based on modules identified by experimental studies and linking these building blocks, we are able to perform computational simulations of signaling networks that may be used to develop novel predictions that can be tested experimentally.

In this chapter we focused on experimentally characterizing the complex mechanisms leading to TNF production. The experimental quantification of these mechanisms was incorporated into mathematical models based on the modules identified for TNF transcription, mRNA stabilization, translation, and secretion that can recapitulate the experimental results and be used in chapter 3 to make predictions about TLR-induced autocrine and paracrine TNF production in the context of NFκB signaling.

Materials and Methods

Animals and cell culture

For all experiments using mice, the C57BL/6 strain was used. These mice were housed at the University of California, San Diego (UCSD) in pathogen-free conditions. The experiments performed using mice were in accordance with protocols authorized by the UCSD Institutional Animal Care and Use Committee. Bone Marrow-Derived Macrophages (BMDMs) were made through the isolation of 6 x 10^6 bone marrow cells from C57BL/6 mouse femur and tibia bones from wild-type, *trif*$^{-/-}$, *myd88*$^{-/-}$, and *irf3*$^{-/-}$ *irf7*$^{-/-}$ mice. To differentiate into BMDMs, BM cells were cultured in L929-conditioned media for 7 days in 15cm suspension dishes at 37°C and 5% CO_2. On day 7, the differentiated BMDMs were collected and re-plated in Dulbecco's modified Eagle's medium (DMEM) supplemented with 10% fetal bovine serum at a density of either 14.3 x 10^6 cells per 15cm culture dish (nascent TNF mRNA

isolation) or 2 x 10^6 cells per 6cm culture dish (all other experiments). Fetal Liver Derived Macrophages (FLDMs) were isolated from the fetal liver of E13-E14 embryos of wild-type or *rela*$^{-/-}$*relb*$^{-/-}$*crel*$^{-/-}$ mice, followed by culturing in L929-conditioned media for 7 days in suspension dishes at 37°C and 5% CO_2. On day 7, the differentiated FLDMs were collected and re-plated in Dulbecco's modified Eagle's medium (DMEM) supplemented with 10% fetal bovine serum.

Analysis of Secreted TNF

For all ELISA experiments to measure the concentration of secreted TNF, BMDMs were replated on day 7 at a density of 2 x 10^6 cells per 6cm culture dish in DMEM supplemented with 10% fetal bovine serum. On day 8, BMDMs were stimulated with 10ng/mL of LPS (Sigma, B5:055) in 1mL of DMEM media per plate. After stimulation for each indicated time, the media from each plate was collected and stored at -20°C until processed. To measure the concentration of TNF secreted by BMDMs into the media, ELISAs were performed using the mouse TNF alpha ELISA Ready-SET-Go!® kit in Corning Costar 9018 high affinity binding 96-well plates (affymetrix eBioscience cat #88-7324-77). TNF concentration in cell media was measured in triplicate wells and incubated overnight at 4°C. Standard solutions of 2-fold dilutions of 1000pg/mL mouse TNF standard down to 7.5pg/mL were used and a standard curve applied as in the manufacturer's guidelines. ELISA 96-well

plates were read using a BioTek Epoch Micro-Volume Spectrophotometer System.

RNA extraction and cDNA preparation

For all mRNA analysis, BMDMs and FLDMs were replated on day 7 at a density of 2 x 10^6 cells per 6cm culture dish in DMEM supplemented with 10% fetal bovine serum. On day 8, BMDMs were stimulated with 10ng/mL LPS in 1mL of DMEM media per plate, while FLDMs were stimulated with 100ng/mL LPS. To isolate RNA for mature mRNA analysis, the plates were washed with ice-cold PBS+1mM EDTA and total RNA was extracted using Qiagen QIAshredder and RNeasy kits according to the manufacturer's guidelines (Qiagen). RNA was eluted with 30µL of RNase-free water and stored at -80°C. cDNA libraries were created from 500ng of total RNA using the Bio-Rad iScript cDNA synthesis kit per the manufacturer's instructions (Bio-Rad).

For all nascent mRNA analysis, BMDMs were replated on day 7 at a density of 14.3 x 10^6 cells per 15cm culture dish in DMEM supplemented with 10% fetal bovine serum. On day 8, BMDMs were stimulated with 10ng/mL of LPS in 10mL of DMEM media per plate. All steps were performed on ice or at 4°C. Cells were washed with ice-cold PBS+1mM EDTA and lysis buffer (10 mM Tris pH 7.5, 150mM NaCl 0.5 mM EDTA pH 8.0, 0.15% NP-40, 1 mM DTT, 1 mM PMSF, 10 µg/ml aprotinin, 5 µg/ml leupeptin, and 1mM pepstatin)

added to plates to lyse cytoplasmic membranes. Nuclei pellets were formed by applying to a 675µL cushion of 0.9M sucrose in lysis buffer followed by centrifugation at 11,700g for 10min. Resulting nucleoplasmic pellets were washed with ice-cold PBS+1mM EDTA and resuspended in 600µL of glycerol buffer (20mM Tris pH 7.9, 75mM NaCl, 50% Glycerol, 0.5mM EDTA, 1mM DTT, 1 mM PMSF, 10 µg/ml aprotinin, 5 µg/ml leupeptin, and 1mM pepstatin). Then, 600µL of nuclei lysis buffer (10mM HEPES pH 7.6, 75mM $MgCl_2$, 0.3mM NaCl, 1mM Urea, 0.2mM EDTA, 1% NP-40, 1 mM DTT, 1 mM PMSF, 10 µg/ml aprotinin, 5 µg/ml leupeptin, and 1mM pepstatin) was added to each sample and vortexed. Samples were centrifuged for 2 minutes at 11,700g, leaving the chromatin pellet. The chromatin pellet was washed with ice-cold PBS+1mM EDTA followed by the addition of 1mL TRIzol reagent (Life Technologies). 0.2mL of cloroform was added to each sample and shaken vigorously for 20 seconds. Samples were centrifuged for 15 minutes at 12,000g at 4°C. The RNA-containing aqueous phase was removed and an equal volume of 70% ethanol added. The resulting solution containing chromatin RNA was purified using the RNeasy kit in 30µL of RNase-free water according to the manufacturer's guidelines (Qiagen).

The purified RNA was then treated with DNase to remove any DNA from the sample preparation by mixing 500ng-1µg of RNA with DNase I, DNase I buffer, and RNase inhibitor (RNase Out) and incubating at room temperature for 20 minutes. EDTA was then added to a final concentration of

2.25mM and samples heated at 65°C for 10 minutes. The chromatin RNA samples with digested DNA were then used to make cDNA libraries using the iScript cDNA synthesis kit according to the manufacturer's guidelines (Bio-Rad).

qRT-PCR

In order to measure the nascent and mature mRNA expression levels of TNF and two housekeeping genes, GAPDH and actin, quantitative real-time PCR (RT-PCR) was used. For mature mRNA expression level analysis, primers for TNF and the housekeeping gene GAPDH were designed (TNF: 5'-CACCACGCTCTTCTGTCTAC forward, 5'-AGAAGATGATCTGAGTGTGAGG reverse; GAPDH: 5'-AACTTTGGCATTGTGGAAGG forward, 5'-GGATGCAGGGATGATGTTCT reverse). For nascent mRNA expression level analysis, primers for nascent TNF mRNA and actin were designed to bind regions that span intron-exon junctions or intronic regions (ntTNF: 5'-CCCAGACCCTCACACTCAGTA forward, 5'-AACTGCCCTTCCTCCATCTT reverse; ntActin: 5'- CTGTATTCCCCTCCATCGTG forward, 5'-GCTTGCCACTCCCAAAGTAA reverse). As nascent mRNA, but not mature mRNA, contains intronic regions or junctions, the amplified qRT-PCR signal can be related to nascent mRNA expression levels. Samples were analyzed in triplicate in 384 PCR plates using 1.0 µl cDNA template, 1.0 µl (100 nM final concentration) of each primer, and 2.5 µl SsoAdvanced SYBR Green

Supermix (Bio-Rad). qRT-PCR was performed on a Bio-Rad CFX384 Real-Time Detection System and analyzed using the Bio-Rad CFX Manger Software v1.6, with amplification of genes of interest represented in quantifaction cycle (Cq) values. Fold changes (represented on log2 and linear scales) for all time points within experiments are relative to the wild-type 0-hr timepoint, calculated by the Δ(ΔCq) method previously described (Schmittgen and Livak, 2008).

TNF half-life determination

For the collection of mRNA for the determination of TNF half-life, BMDMs were replated on day 7 at a density of 2 x 10^6 cells per 6cm culture dish in DMEM supplemented with 10% fetal bovine serum. On day 8, BMDMs were stimulated with 10ng/mL TNF alone or with a combination of 10ng/mL TNF and 10ng/mL LPS in 1mL of DMEM media per plate. After 30 minutes of stimulation, actinomycin-d (Sigma), a drug that intercalates into DNA and arrests transcription, was added to each plate at a final concentration of 10nM. Time points were collected in 15-minute increments up to 60 minutes following actinomycin-d treatment. RNA extracts were collected and purified, cDNA libraries were synthesized, and qRT-PCR was analyzed as previously described. The half-life of TNF mRNA was determined by graphing TNF mRNA expression levels relative to the timepoint taken at time 0 of

actinomycin-d treatment, and a trendline applied. The half-life was calculated by taking the inverse of the slope of these trendlines multiplied by *ln*(2).

Nuclear extraction and gel shift assays

BMDMs were replated on day 7 at a density of 2 x 10^6 cells per 6cm culture dish in DMEM supplemented with 10% fetal bovine serum. On day 8, BMDMs were stimulated with 10ng/mL of LPS in 1mL of DMEM media per plate. CE Buffer (10mM HEPES pH 7.9, 10mM KCl, 0.1mM EGTA, 0.1mM EDTA, 1mM DTT, 1mM PMSF, 10µg/ml aprotinin and 5µg/ml leupeptin) was added to plates to collect cells. 0.5% NP-40 was then added to each sample and vortexed. Nuclei pellets were formed by centrifugation at 4000g for 1 minute, followed by resuspension of nuclei pellets in 15µL of nuclear extract buffer (20 mM HEPES ph 7.9, 400mM NaCl, 1.5mM $MgCl_2$, 0.2mM EDTA, 25% glycerol, 1mM DTT, 1mM PMSF, 10µg/ml aprotinin and 5µg/ml leupeptin). The nuclear lysates were centrifuged at 14,000g at 4°C for 5 minutes, and protein concentrations determined by Bradford assay (Bio-Rad). Nuclear lysates from each experiment were normalized, and Electrophoretic Mobility Shift Assays (EMSAs) performed as described previously (Werner et al., 2005). Nuclear lysates were incubated at room temperature for 15 minutes with a P^{32}-labelled HIV G1G2 probe, a double-stranded oligonucleotide that contains two κB sites:

(GCTACAAGGGACTTTCCGCTGGGGACTTTCCAGGGAGG). Samples were applied to and run on a non-denaturing acrylamide gel to separate bands corresponding to activated NFκB binding the κB-containing P^{32}-labelled probe. These bands were captured by audioradiography and analyzed using ImageQuant software (GE Lifesciences). Quantification of bands was performed by measuring the absolute intensity of each p65-p50 NFκB dimer band and normalizing all intensities to the peak wild-type band intensity.

Immunobloting

For immunoblot analysis, BMDMs were replated on day 7 at a density of 2 x 10^6 cells per 6cm culture dish in DMEM supplemented with 10% fetal bovine serum. On day 8, BMDMs were stimulated with 10ng/mL of LPS in 1mL of DMEM media per plate. For drug treatments with inhibitors for p38 and ERK, cells were treated with DMSO alone, 10μM p38 inhibitor in DMSO, or 10μM ERK inhibitor in DMSO for 1 hour prior to stimulation with LPS (p38: SB 203580 Tocris; ERK1/2: FR180204 Sigma). After stimulation, cells were washed with PBS+1mM EDTA, and whole-cell extracts prepared using RIPA buffer (50mM Tris pH 7.5, 150mM NaCl, 1mM EDTA, 0.1% SDS, 1.0% Triton X-100, 1mM DTT, 1mM PMSF, 10μg/ml aprotinin, 5μg/ml leupeptin, 1mM $NaVO_4$, 10mM NaF, 20mM BGP). Protein concentrations were analyzed by Lowry assay. Antibodies used include phospho-p38 Thr180/Tyr182 (Cell Signaling Rabbit mAb #4511), phospho-ERK1/2 Thr202/Tyr204 (Cell Signaling

Rabbit mAb #4370), phospho-MK2 Thr334 (Cell Signaling Rabbit mAb #3007), phospho-MK2 Thr222 (Cell Signaling Rabbit mAb #3316), phospho-TTP Ser178 (A gift from Dr. Paul Anderson at Brigham and Women's Hospital), TNF (Cell Signaling Rabbit mAb #3042), phospho-eIF4E Ser209 (Cell Signaling Rabbit #9741), phospho-TACE Thr735 (Abcam Rabbit ab60996, Assay Biotech Rabbit A0763), and actin (Santa Cruz Goat sc-1615).

Computation Simulations

Simple Ordinary Differential Equations (ODEs) were written for each step in the production of TNF (nascent gene transcription, mRNA half-life stabilization, translation/secretion) based on the modules identified through experimental approaches. Experimentally derived values of inputs and outputs for each mathematical model were used in parameterization. For TRIF-mediated TNF mRNA half-life begins at 17 minutes, linearly increases upon stimulation to 37 minutes following 30 minutes of stimulation, and then decreases linearly to 10 minutes of half-life after 1 hour of stimulation. The three TNF production models were then connected, where the output of one model serves as the input for the subsequent model. The fitness of each mathematical model to math experimental data was determined and scored by RMSD. MATLAB version R2013a (The MathWorks Inc.) was used to numerically solve ODEs with the subroutine *ode15s.*

Dynamics of TNF production are dependent on kinetics of TRIF and MyD88-mediated signaling events

To investigate the TRIF- and MyD88-specific control mechanisms and temporal dynamics of TNF production in TLR signaling, we used the TLR agonist that activates both TRIF and MyD88: lipopolysachharide (LPS). First, we measured TNF secretion in the supernatant of LPS-stimulated wild-type, *trif*$^{-/-}$, and *myd88*$^{-/-}$ BMDMs. This revealed that while both *trif*$^{-/-}$ and *myd88*$^{-/-}$ have significant defects in TNF secretion, *trif*$^{-/-}$ BMDMs surprisingly exhibited even lower TNF secretion than *myd88*$^{-/-}$ (Fig 2.1A). To determine whether the defects in TNF secretion seen in *trif*$^{-/-}$ and *myd88*$^{-/-}$ is due to decreased mRNA production, BMDMs were stimulated with LPS and mature mRNA levels were measured (Fig 2.1B). Unsurprisingly, *myd88*$^{-/-}$ had decreased mature TNF mRNA production compared to wild-type, showing no early mRNA production within 30 minutes, and reaching its peak around 1 hour. However, *trif*$^{-/-}$ BMDMs had only a small defect in mature TNF mRNA production, suggesting that TRIF may control translational or post-translational processing of TNF. To determine the TNF mRNA synthesis rates, wild-type, *trif*$^{-/-}$, and *myd88*$^{-/-}$ BMDMs were stimulated with LPS and nascent transcripts collected. This revealed that while *myd88*$^{-/-}$ showed significantly decreased nascent TNF mRNA for the first 25 minutes of LPS stimulation, nascent TNF mRNA levels were slightly increased above wild-type after 60 minutes of LPS stimulation (Fig 2.1C). In contrast, *trif*$^{-/-}$ BMDMs exhibited slightly increased nascent TNF

mRNA levels over wild-type for the first 30 minutes of LPS stimulation, but decreased compared to wild-type after 60 minutes. The fact that *trif*$^{-/-}$ BMDMs have increased nascent TNF mRNA for the first 30 minutes of LPS stimulation compared to wild-type but decreased total mature mRNA production throughout the time course suggests that TRIF may control post-transcriptional processing of TNF as well.

TNF mRNA production is regulated by NFκB, but not IRF

In addition to leading to the activation of NFκB, the signaling adaptor TRIF also activates the transcription factor IRF3, leading to production of IFN-B and activation of the IFNAR signaling pathway. Previous reports had suggested that in addition to NFκB, IRF3 activation was an important factor in TNF production in response to TLR agonists such as LPS (Covert et al., 2005). To investigate whether TNF gene transcription was controlled by solely NFκB or by IRF3 as well, wild-type and *rela*$^{-/-}$*relb*$^{-/-}$*crel*$^{-/-}$ FLDMs were stimulated with LPS. Here, we found that *rela*$^{-/-}$*relb*$^{-/-}$*crel*$^{-/-}$ FLDMs have no appreciable mature TNF mRNA production, supporting the model that NFκB is essential for TNF gene transcription (Fig 2.2). To investigate whether IRF3 was involved in TNF gene transcription, *irf3*$^{-/-}$*irf7*$^{-/-}$ BMDMs were stimulated with LPS and mature TNF mRNA production measured; this revealed that *irf3*$^{-/-}$*irf7*$^{-/-}$ had no defects in mature TNF mRNA production (Fig 2.3A). To ensure that this was true for nascent TNF mRNA production as well, nascent

transcript analysis in *irf3*$^{-/-}$*irf7*$^{-/-}$ BMDMs stimulated with LPS demonstrated that there is no defect in TNF gene transcription and that IRF3 activation is not needed for TNF production (Fig 2.3B).

As NFκB was confirmed to be the transcription factor solely responsible for TNF transcription, we sought to characterize NFκB activation in *trif*$^{-/-}$ and *myd88*$^{-/-}$ BMDMs in response to LPS; this revealed that NFκB activation is decreased in both *trif*$^{-/-}$ and *myd88*$^{-/-}$ (Fig 2.4). The *trif*$^{-/-}$ BMDMs have normal early activation (0-30 minutes) but significantly decreased activation following 30 minutes; conversely, *myd88*$^{-/-}$ BMDMs have decreased early activation, but late activation (45 minutes to 4 hours) is unchanged compared to wild-type.

A Module for TLR-induced nascent TNF mRNA production

Given that TRIF and MyD88-mediated NFκB activation is what drives the transcription of the TNF gene, we were able to devise a module for nascent TNF RNA production using NFκB activity as an input and nascent TNF mRNA as an output (Fig 2.5). This module serves as a basis for a computation model describing the production of nascent TNF mRNA in the context of LPS-induced NFκB signaling; this model consists of a TNF gene containing two κB sites, where NFκB is able to bind. Upon NFκB binding (the activity of which is determined through quantification of EMSA experiments), nascent TNF RNA is produced, which can be processed into mRNA. In this mathematical model, the rate of nascent TNF transcription can be determined

by a Hill equation based on NFκB activity and promoter binding sites, and a mass action equation for nascent processing. Previous work as shown that PKR activity is important for processing nascent TNF RNA to mRNA(Osman et al., 1999), and that PKR activation is at least partially mediated by MyD88 (Horng et al., 2001). Given that MyD88 and TRIF both contribute to p38 and ERK activation, which are upstream of PKR, in the computational module MyD88 and TRIF equally contribute to nascent RNA processing. Using experimentally determined NFκB activity in LPS-induced signaling as an input, this model is able to recapitulate the experimentally determined nascent TNF RNA transcription seen in WT, *trif*$^{-/-}$, and *myd88*$^{-/-}$ BMDMs.

TRIF controls TNF mRNA half-life

Previous reports have shown that the half-life, translation, and secretion of TNF mRNA can be modulated during TLR signaling. While it is clear that these processes are important for the temporal dynamics of TNF production in TLR signaling, what is not clear is whether MyD88, TRIF, or some combination of the two adaptors controls these regulation steps. The discrepancy between nascent TNF RNA production levels and whole-cell TNF mRNA levels in *trif*$^{-/-}$ BMDMs in response to LPS, prompted us to investigate which stimuli activate the pathways leading to TNF mRNA stabilization, translation, and protein secretion, as well as which TLR adaptor, or combination of both, control these processes.

To investigate the stimulus-specific half-life control of TNF mRNA, wild-type BMDMs were stimulated with TNF alone, which induces TNF mRNA expression but not TNF mRNA stabilization, or TNF and LPS. Following stimulation, treatment with the drug actinomycin-d arrests transcription and allows for the measurement of the rate of decay of TNF mRNA. Stimulation with TNF set a baseline of constitutive TNF mRNA half-life of around 10 minutes (Fig 2.6). When stimulated in conjunction with LPS, the half-life of TNF mRNA increased 3.5 fold to 35 minutes. To determine whether this LPS-induced stabilization of TNF mRNA was TRIF or MyD88-specific, we investigated this *trif*$^{-/-}$ and *myd88*$^{-/-}$ BMDMs as well. This revealed that while the *myd88*$^{-/-}$ showed no decrease in LPS-induced TNF mRNA half-life compared to wild-type, the *trif*$^{-/-}$ cells showed a complete loss of the LPS-induced mRNA stabilization, with a half-life of 10 minutes. This data demonstrates that TRIF, and not MyD88, is necessary for TNF mRNA stabilization in macrophages. To determine whether this stabilization was p38-dependent, 30 minutes prior to LPS stimulation, wild-type BMDMs were treated with p38 inhibitor. After actinomycin-D treatment, p38-inhibitor treated TNF mRNA half-life was determined by qRT-PCR to be around 13 minutes, showing that the TRIF mediates TNF mRNA stabilization through p38.

As p38 and ERK pathways have been implicated in the control of post-transcriptional processing of TNF mRNA, and both TRIF and p38 are essential for stabilization of TNF mRNA, we sought to characterize the activation of the

p38 and ERK pathways. Immunoblots for phopsho-p38 and phospho-ERK in LPS stimulated wild-type, *trif*$^{-/-}$, and *myd88*$^{-/-}$ BMDMs were performed within a window of 30-90 minutes after LPS stimulation (the timeframe where the mRNA half-lives were measured) (Fig 2.7). This revealed that from 30 to 75 minutes, *trif*$^{-/-}$ BMDMs have decreased p38 activation. Similarly, while ERK activation dynamics are more transient than p38 activation dynamics, *trif*$^{-/-}$ BMDMs showed decreased ERK activation from 30-60 minutes. Given that previous reports had showed that the MAPK target MK2 is important for TNF mRNA stabilization and translation, we performed immunoblots for phospho-MK2 as well. This revealed that while the *myd88*$^{-/-}$ may have slightly decreased activity at 30 minutes only, the *trif*$^{-/-}$ have decreased MK2 activity from 30-60 minutes. To determine whether this MK2 phosphorylation is p38 or ERK-dependent, WT BMDMs were pre-treated with p38 or ERK inhibitor for 1 hour prior to LPS stimulation, and immunoblots for phospho-MK2 performed (Fig 2.8). This revealed that p38, and not ERK, is essential for MK2 activation, as p38 inhibition completely abolished phosphorylation of MK2, while ERK inhibition had no effect. Previous reports have shown that the MK2 target TTP is a primary regulator of TNF mRNA degradation. We found that phosphorylation of TTP, which leads to its inactivation and prevents TNF mRNA degradation, is decreased in p38-inhibitor treated wild-type BMDMs stimulated with LPS, but not significantly in ERK-inhibitor treated cells.

A module for TRIF-mediated TNF mRNA stabilization

These mechanistic insights concerning the TRIF-mediated control of TNF mRNA stabilization were incorporated into a simple module for TNF mRNA half-life control, whereby TRIF leads to the activation of p38, p38 phosphorylates and activates MK2, and MK2 phosphorylates TTP which prevents TTP from binding the 3' ARE elements in TNF mRNA, leading to the stabilization of the TNF message and an increase in half-life (Fig 2.9). A computational model based on this half-life control module uses the experimentally determined nascent TNF RNA levels as input, and outputs mature TNF mRNA. The effect of TNF mRNA stabilization can be illustrated by contrasting the output of total TNF mRNA simulations for four potential half-life control mechanisms. Here, root-mean-square deviation scoring (RMSD) reveals that the TRIF-controlled scenario best recapitulates the experimental data, confirming that although *trif*$^{-/-}$ have increased nascent TNF RNA levels compared to wild-type, they have slightly decreased mRNA levels.

TRIF accelerates translation and secretion of TNF mRNA

While post-transcriptional control of TNF mRNA stabilization by TRIF accounts for the discrepancy between nascent TNF RNA and mature TNF mRNA levels in *trif*$^{-/-}$ BMDMs, these cells still show a significant lack of TNF secretion compared to wild-type cells that is not apparent at the level of mRNA production. In order to characterize adaptor-specific control TNF translation,

immunoblots for pro-TNF expression were carried out in wild-type, *trif*$^{-/-}$, and *myd88*$^{-/-}$ BMDMs pre-treated with TACE inhibitor TAPI-1 to block secretion and stimulated with LPS. This revealed that while wild-type macrophages produce significant amounts of pro-TNF peaking at 60 minutes, *trif*$^{-/-}$ and *myd88*$^{-/-}$ cells have serious defects in pro-TNF expression (Fig 2.10). While *myd88*$^{-/-}$ BMDMs show little to no TNF mRNA induction at 30 minutes so the lack of pro-TNF protein expression at 60 minutes is unsurprising, *trif*$^{-/-}$ have severely decreased pro-TNF expression, demonstrating that TRIF regulates the translation of TNF as well. We sought to determine whether this regulation of translation by TRIF was mediated through p38 or ERK. Wild-type BMDMs were pre-treated with TACE inhibitor and either DMSO, p38 inhibitor, or ERK inhibitor for 1 hour followed by LPS stimulation. The immunoblot for pro-TNF shows that TRIF control of translation is exerted through p38 and not ERK, as the ERK-inhibitor condition showed no decrease in pro-TNF expression (Fig 2.11).

Given that eIF4E and TACE have been shown to be necessary for TNF translation (Andersson and Sundler, 2006) and secretion (Black et al., 1997), respectively, we next sought to characterize their activation. Previous reports have demonstrated that phosphorylation of eIF4E and TACE is necessary for their processive activities (Díaz-Rodríguez et al., 2002; Fan and Derynck, 1999; Topisirovic et al., 2004; Wang et al., 1998; Xu and Derynck, 2010). Wild-type, *trif*$^{-/-}$, and *myd88*$^{-/-}$ BMDMs were stimulated with LPS and immunoblots

for phospho-eIF4E and phospho-TACE performed (Fig 2.12A). Here, *myd88*$^{-/-}$ macrophages show decreased eIF4E phosphorylation around 30-45 minutes, while *trif*$^{-/-}$ cells show significantly decreased eIF4E phosphorylation from 60-75 minutes. While both adaptors contribute to TNF translation, the levels of TNF mRNA able to be translated are significantly lower at 30 minutes, where MyD88 primarily contributes to eIF4E activity, than at 60 minutes, where TRIF primarily contributes to eIF4E activity. Further, immunoblots for TACE phosphorylation were performed. While wild-type and *myd88*$^{-/-}$ cells exhibited significant TACE phosphorylation, peaking at 75 minutes, the *trif*$^{-/-}$ cells showed decreased TACE phosphorylation in comparison. To determine whether TRIF-controlled phosphorylation of TACE was mediated through p38 or ERK MAPK, wild-type BMDMs were pre-treated with p38 or ERK inhibitor for one hour, followed by stimulation with LPS (Fig 2.12B). This revealed that both p38 and ERK have an effect on TACE phosphorylation, but ERK is essential. While pre-inhibition of p38 decreased TACE phosphorylation modestly, ERK pre-inhibition eliminated TACE phosphorylation completely.

A module for TRIF-mediated promotion of TNF translation and secretion

These experimental results led us to the characterization of a module for the control of TNF translation and secretion. In this module, TRIF leads to the activation of p38 and ERK pathways; p38 controls the activity of eIF4E through phosphorylation, which promotes TNF translation, whereas ERK and

p38 controls the activity of TACE through phosphorylation, which promotes the cleavage and secretion of TNF (Figure 2.13). We then constructed a mathematical model based on this module architecture, using experimentally determined LPS-induced mRNA levels as an input and secreted TNF protein as an output, including experimentally determined pro-TNF as an intermediate within the model. This allows us to perform computational simulations to investigate the role that TRIF plays in promoting TNF translation and TNF secretion (Fig 2.13). Simulating the model with and without TRIF-mediated control of TNF translation and secretion demonstrates that TRIF-mediated control of translation and secretion is indeed necessary to recapitulate the experimentally determined levels of both pro-TNF expression and TNF secretion.

Discussion

Macrophages play an early, key role in the innate immune response to a variety of pathogens through the activation of TLRs. The regulation of TNF production in response to PAMPs is a dynamic process, and a quantitative understanding of the temporal kinetics of TNF production can be informative for how the cytokine acts in autocrine and paracrine manners. In this chapter, we investigated the mechanisms leading to the production of TNF and used the biochemical insights gained to build mathematical models based on modules identified for each step in TNF production.

While there have been many reports concerning the mechanisms by which TNF production is modulated in response TLR agonists, the cell systems used were diverse; as a result, it was unclear whether these mechanisms were stimulus-specific or whether they were controlled by TRIF or MyD88 in macrophages. We demonstrate that while MyD88 is primarily responsible for early nascent TNF RNA induction as well as TNF mRNA production, TRIF is essential for the activation of post-transcriptional mechanisms that promote the processing of TNF: mRNA stabilization, pro-TNF translation, and TNF secretion. Stabilization of TNF mRNA, leading to the increase in TNF mRNA half-life, is controlled through a TRIF-p38-pMK2 axis whereby TRIF leads to the activation of MAP kinases which downregulate mRNA degradation mechanisms. Further, the translation of TNF mRNA to pro-TNF is shown to be controlled by TRIF, as TRIF-deficient macrophages have significantly decreased pro-TNF expression compared to predicted levels, given the relatively high levels of TNF mRNA seen in TRIF-deficient cells. At the level of TNF secretion, the enzyme TACE has been previously shown to cleave membrane-bound pro-TNF, and that it is controlled by p38 and ERK. Here, we confirm that both p38 and ERK activity are needed for proper TACE activation, and that TACE activation is primarily controlled by TRIF. These three TRIF-controlled post-transcriptional mechanisms are essential for proper temporal kinetics of TNF production in response to LPS, as a deficiency in TRIF leads cells to secrete significantly less TNF protein despite their near-

wild-type levels of TNF mRNA.

In this chapter, we characterize TNF production in three discrete modules: transcription, mRNA stabilization, and translation/secretion. The architecture for these individual modules has been developed by investigating and quantifying stimulus-specific (LPS) and adaptor-specific (MyD88, TRIF) mechanisms. The mathematical models based on these modules have been parameterized using experimental kinetic values of inputs and outputs, such that they can recapitulate experimental results. One major advantage of using a modular, computational approach based on experimental insights to characterize TNF production mechanisms is that the computational approach provides a confirmation of the experimental mechanisms. For example, in the case of mRNA stabilization, experimental data suggests TRIF controls TNF mRNA half-life; when using a computational model with experimentally determined nascent mRNA as an input and mature mRNA as an output, the only adaptor-mediated control scenario that is able to recapitulate the experimental mature mRNA levels is by TRIF. This dual approach blending experiment and simulation engenders confidence in the results that neither approach alone provides. Furthermore, with the simple topology and input/outputs of these modules, they can be connected to form larger signaling networks that can be used to make useful predictions about functions within the network. In Chapter 3, the three TNF production modules will be joined with previously published TNFR, TLR, and IKK/NFκB modules to create a

mathematical model of the TNF signaling network downstream of TLRs and that can be used to make predictions about the autocrine and paracrine signaling functions of TNF.

Acknowledgements

Chapter 2, is a modified presentation of material that is being prepared for publication as “Network dynamics determine the autocrine and paracrine signaling functions of TNF” by Caldwell AB, Cheng Z, Vargas A, Birnbaum H, and Hoffmann A. The dissertation author was the primary investigator and author of this material. Zhang Cheng performed the mathematical modeling and computational simulations. Christine Cheng provided RNA from LPS-stimulated FLDMs for mature mRNA analysis.

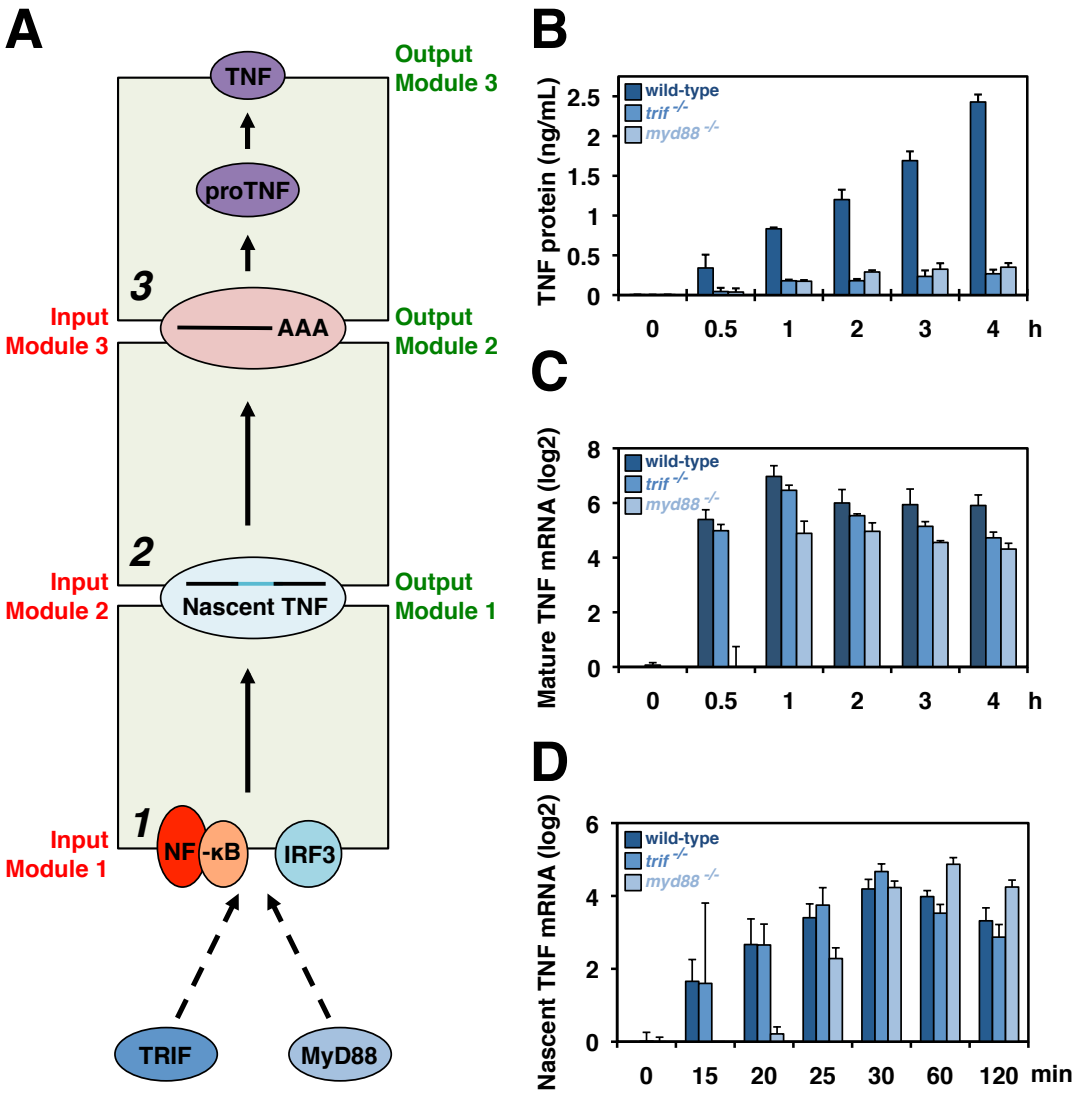

Figure 2.1 TRIF and MyD88 Contribute to TNF production
A Diagram of the three TNF production modules investigated **B** Secretion of TNF in cell media measured by ELISA in wild-type, *trif* $^{-/-}$, or *myd88*$^{-/-}$ Bone Marrow Derived Macrophages (BMDMs). Cells stimulated with 10ng/mL LPS, n=3. **C** Levels of mature TNF mRNA (log2 fold) produced by wild-type, *trif*$^{-/-}$, or *myd88*$^{-/-}$ BMDMs stimulated with 10ng/mL LPS, measured by RT-PCR. Wild-type, n=5. *trif*$^{-/-}$, n=3. *myd88*$^{-/-}$, n=3. **D** Levels of nascent TNF mRNA (log2 fold) produced by wild-type, *trif*$^{-/-}$, or *myd88*$^{-/-}$ BMDMs stimulated with 10ng/mL LPS, measured by RT-PCR. Wild-type, n=3. Nascent transcripts measured by qRT-PCR with intron-exon spanning primers. Error bars indicate 1 standard deviation from the mean of biological replicates.

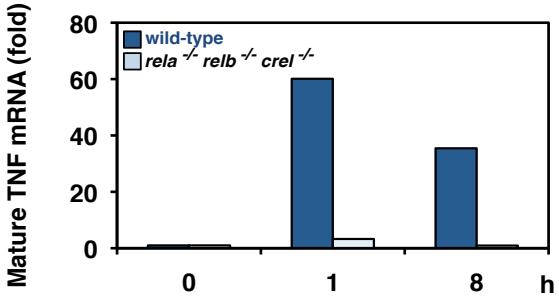

Figure 2.2 NFκB is essential for TNF mRNA production
TNF mRNA levels (fold) measured by qRT-PCR in wild-type or *rela*$^{-/-}$*relb*$^{-/-}$*crel*$^{-/-}$ Fetal Liver Derived Macrophages (FLDMs) stimulated with 100ng/mL LPS (n=1).

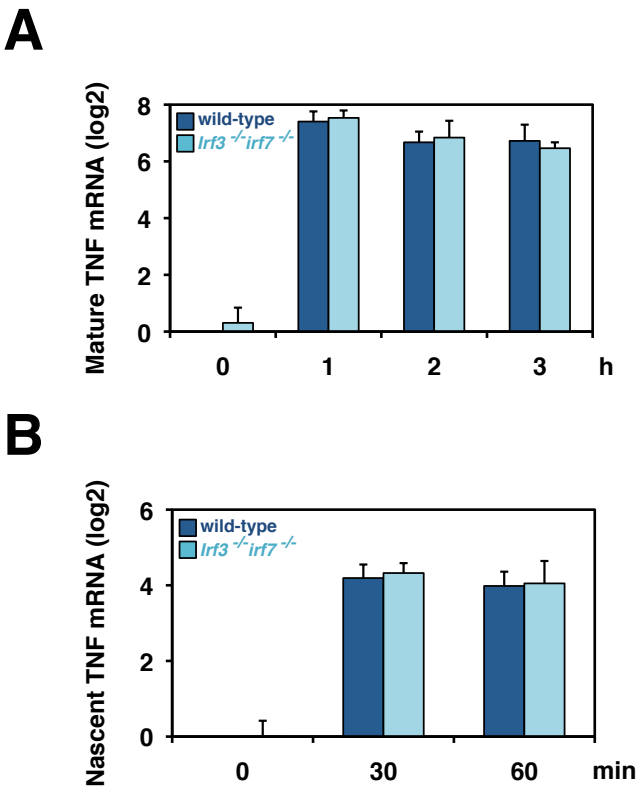

Figure 2.3 IRF3 and IRF7 are dispensible for TNF gene transcription and mRNA production

A Mature TNF mRNA levels (log2) measured by qRT-PCR in Wild-type or *irf3*$^{-/-}$*irf7*$^{-/-}$ BMDMs stimulated with 10ng/mL LPS. **B** Nascent TNF mRNA levels (fold) measured qRT-PCR in Wild-type or *irf3*$^{-/-}$*irf7*$^{-/-}$ BMDMs stimulated with 10ng/mL LPS.

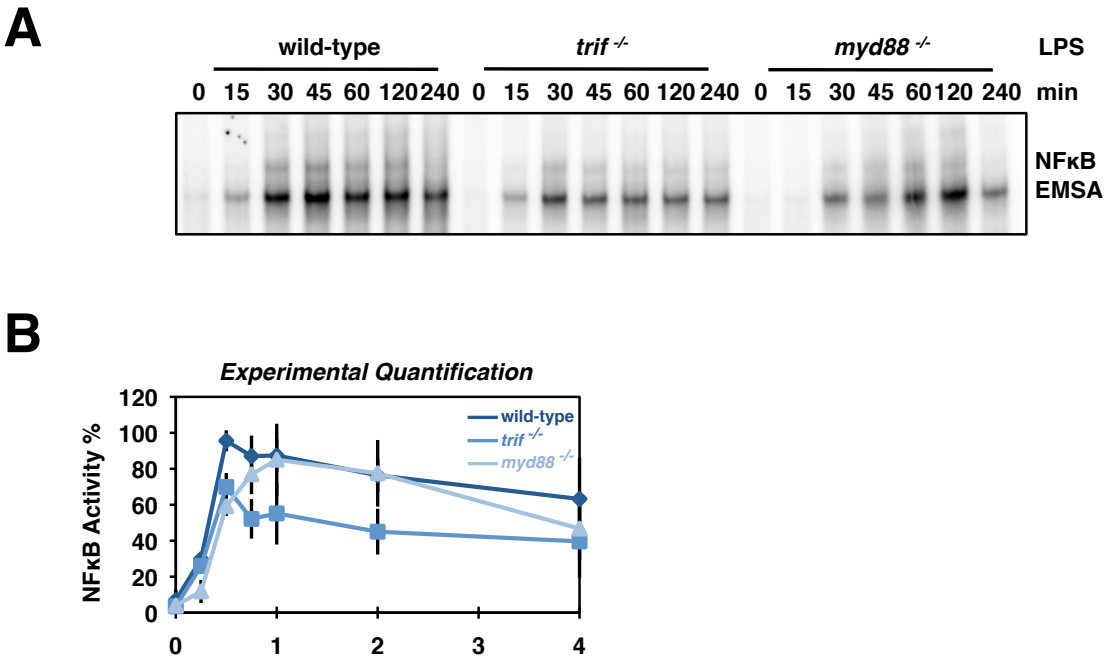

Figure 2.4 MyD88 controls early NFκB activation, TRIF controls late activation

A Activation of NFκB measured by EMSA (G1G2 κB-containing HIV probe) in wild-type, *trif* $^{-/-}$, or *myd88*$^{-/-}$ BMDMs stimulated with 10ng/mL LPS. Arrow indicates p65-p50 dimer. **B** Quantification of NFκB EMSA bands normalized to peak activity (n=3).

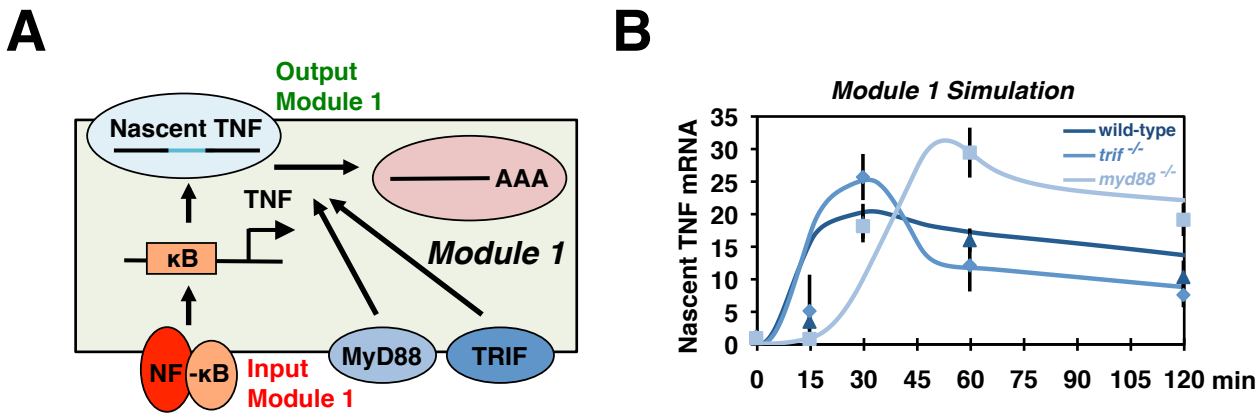

Figure 2.5 A module for nascent TNF mRNA production
A Schematic module for transcription of nascent TNF RNA; for mathematical model, input is quantified NFκB activation data from 2.4B, output is nascent TNF RNA. **B** Lines: computational simulations of the mathematical model for nascent TNF in wild-type, trif$^{-/-}$, or *myd88*$^{-/-}$ genotypes stimulated by 10ng/mL LPS. Data points: experimental data for nascent TNF mRNA in wild-type, *trif* $^{-/-}$, or *myd88*$^{-/-}$ BMDMs stimulated with 10ng/mL LPS as reported in Figure 2.1C

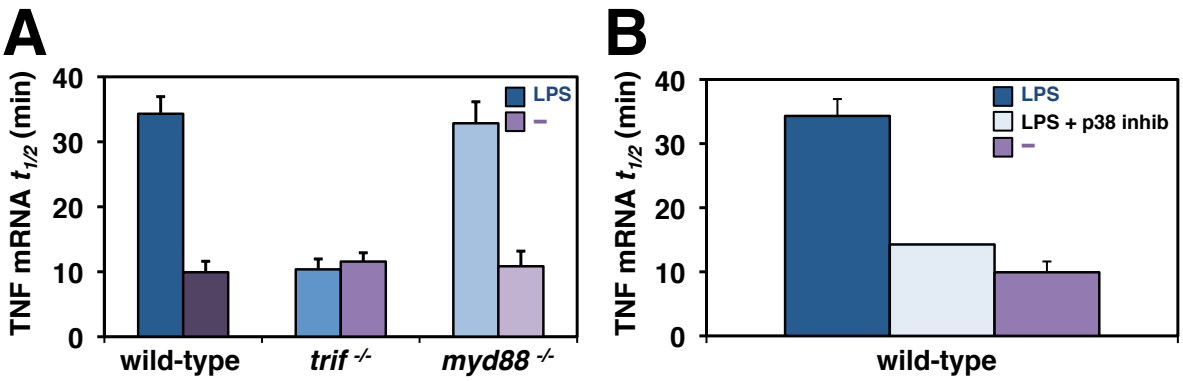

Figure 2.6 TRIF controls TNF mRNA stability
A TNF mRNA half-life measure by RT-PCR. wild-type, *trif* $^{-/-}$, or *myd88*$^{-/-}$ BMDMs pre-stimulated for 30 min with 10ng/mL TNF alone (-) or 10ng/mL TNF and 10ng/mL LPS (LPS) and then treated with actinomycin-d to arrest transcription (wild-type, n=5; *trif* $^{-/-}$, n=4; *myd88*$^{-/-}$, n=3). **B** TNF mRNA half-life measure by qRT-PCR in wild-type BMDMs. Cells pre-stimulated with 10ng/mL TNF alone (-), 10ng/mL TNF and 10ng/mL LPS (LPS), or 10ng/mL TNF, 10ng/mL LPS, and 10μM p38-inhibitor for 30 min, followed by actinomycin-d treatment (TNF, n=5; LPS, n=5; p38, n=1).

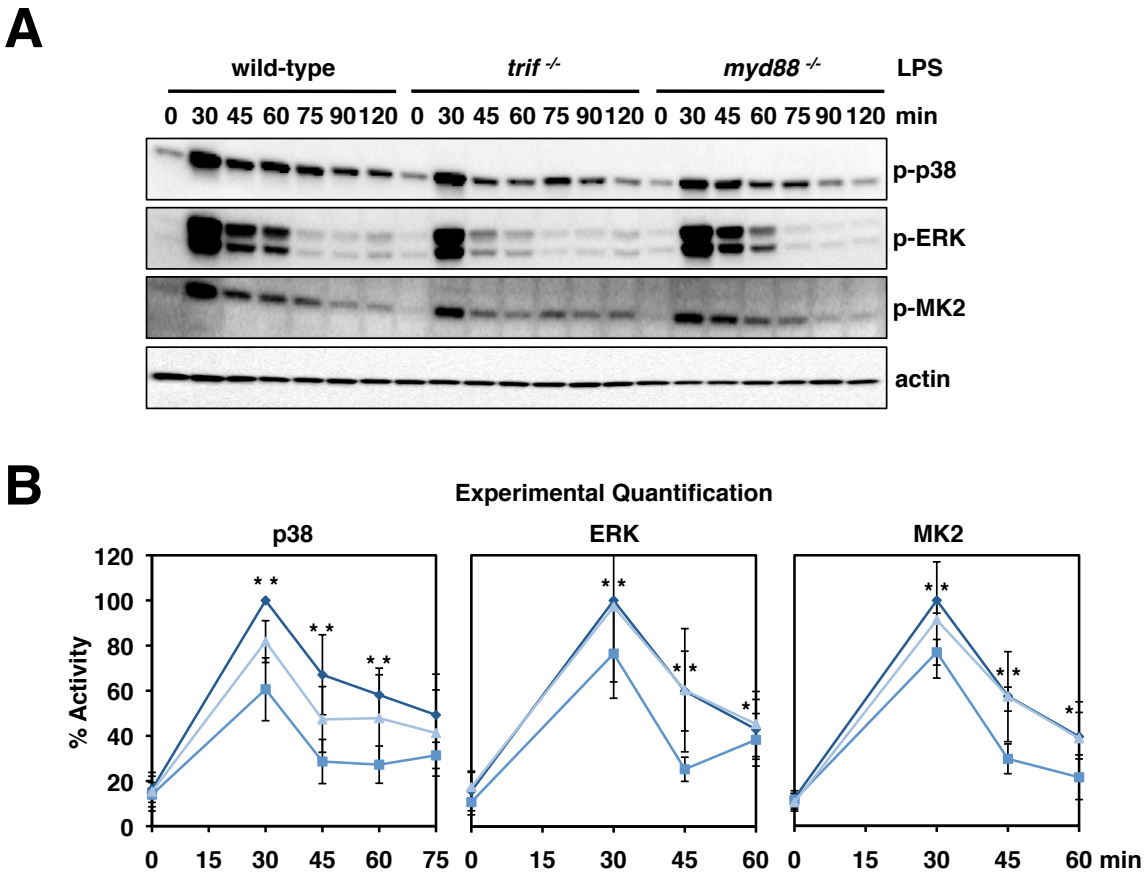

Figure 2.7 TRIF controls p38, ERK, and MK2 activation
A Immunoblots for phospho-p38, phospho-ERK, phospho-MK2, and actin in wild-type, *trif* $^{-/-}$, or *myd88*$^{-/-}$ BMDMs stimulated with 10ng/mL LPS. Blots shown representative of >3 experiments. **B** Quantification of immunoblots normalized to wild-type peak phosphorylation. Error bars indicate 1 standard deviation; * indicates a p value < 0.05, ** indicates a p value < 0.02 for difference between wild-type and *trif* $^{-/-}$ timepoints.

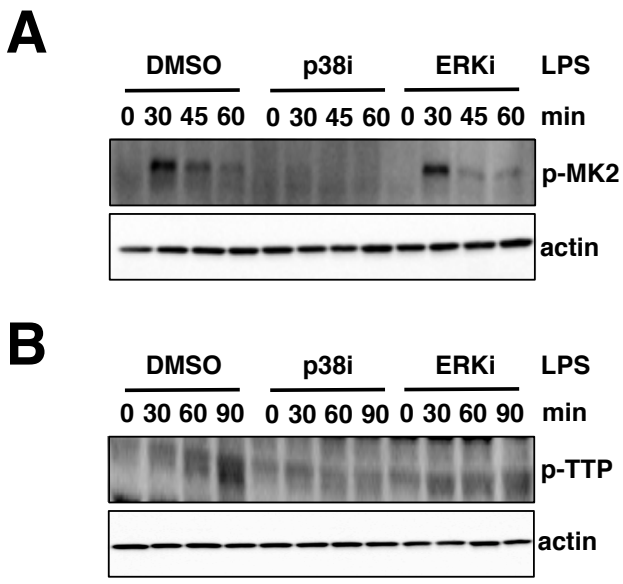

Figure 2.8 p38 controls MK2 and TTP phosphorylation
A Immunoblots of phospho-MK2 and actin in wild-type BMDMs pre-treated with DMSO, 10μM p38 inhibitor, or 10μM ERK inhibitor for 1 hour followed by stimulation with 10ng/mL LPS. **B** Immunoblot for phospho-TTP and actin in wild-type BMDMs pre-treated with DMSO, 10μM p38 inhibitor, or 10μM ERK inhibitor for 1 hour followed by stimulation with 10ng/mL LPS (A, representative of 2 experiments; B, representative of 2 experiments).

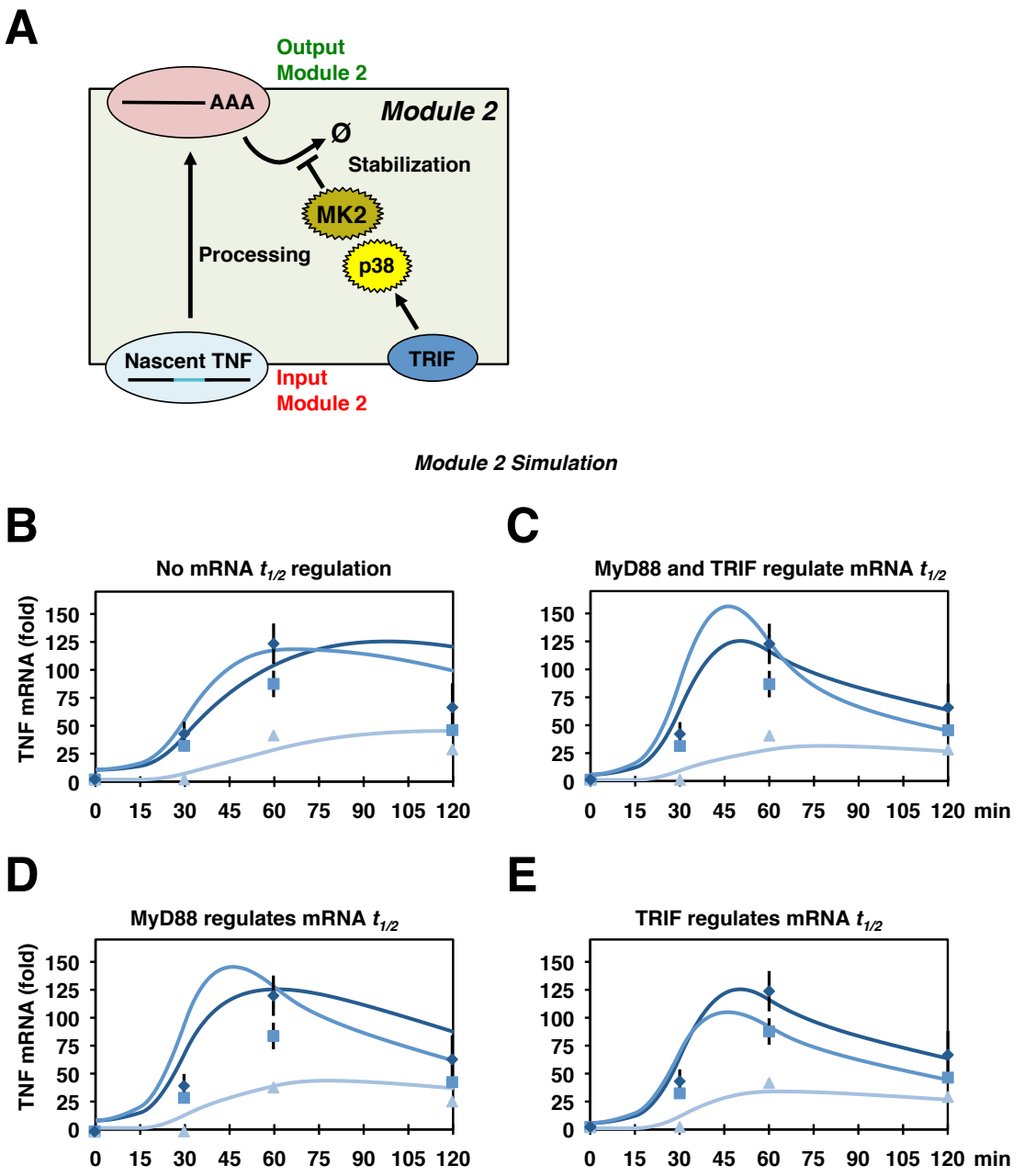

Figure 2.9 A module for TRIF-mediated mRNA half-life stabilization
A Schematic of the module 2 for TRIF-mediated stabilization of TNF mRNA; input: nascent TNF RNA from simulations of module 1; output: mature TNF mRNA. Lines: simulations of module 2 for TNF mRNA production in the wild-type, *trif* $^{-/-}$, or *myd88*$^{-/-}$ genotype in response to 10ng/mL LPS with either **B** no stabilization control, **C** stabilization by TRIF and MyD88, **D** stabilization by MyD88 alone, or **E** stabilization by TRIF alone. Data points: experimental data for mature TNF mRNA in wild-type, *trif* $^{-/-}$, or *myd88*$^{-/-}$ BMDMs stimulated with 10ng/mL LPS as reported in Figure 2.1C.

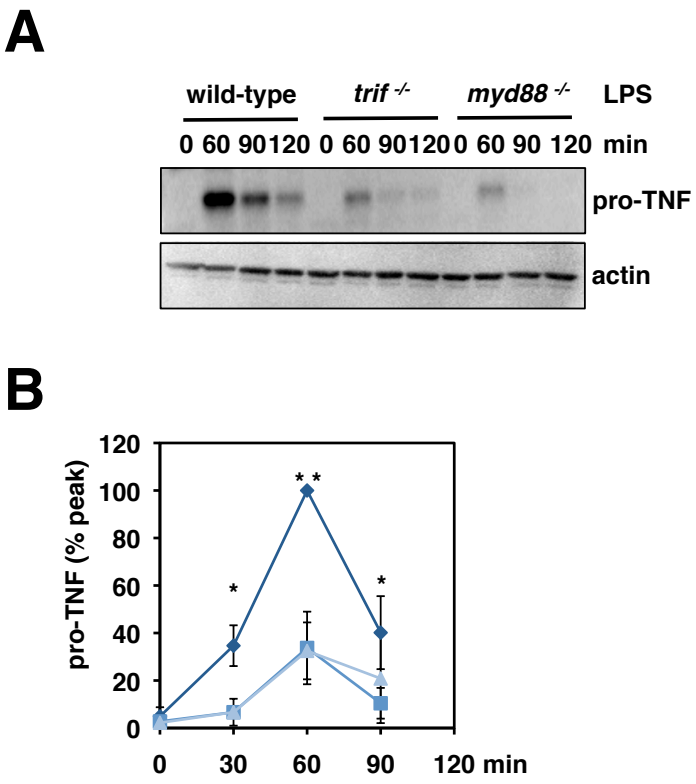

Figure 2.10 TRIF have significantly decreased pro-TNF expression
A Immunoblot for proTNF and actin in wild-type, *trif* $^{-/-}$, and *myd88*$^{-/-}$ BMDMs stimulated with 10ng/mL. Data representative of 3 experiments. **B** Quantification of proTNF bands normalized to peak wild-type protein levels. Error bars indicate 1 standard deviation; * indicates a p value < 0.05, ** indicates a p value < 0.02 for difference between wild-type and trif-/- timepoints.

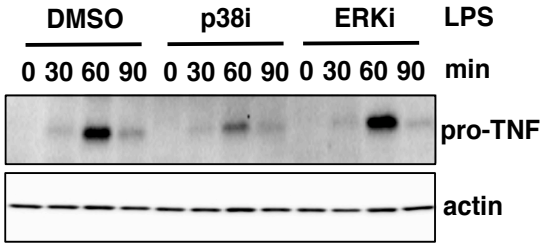

Figure 2.11 p38 controls pro-TNF translation
Immunoblot for proTNF and actin in wild-type BMDMs pre-treated with DMSO, 10μM p38 inhibitor, or 10μM ERK inhibitor for 1 hour followed by stimulation with 10ng/mL LPS. Blot is representative of 2 experiments.

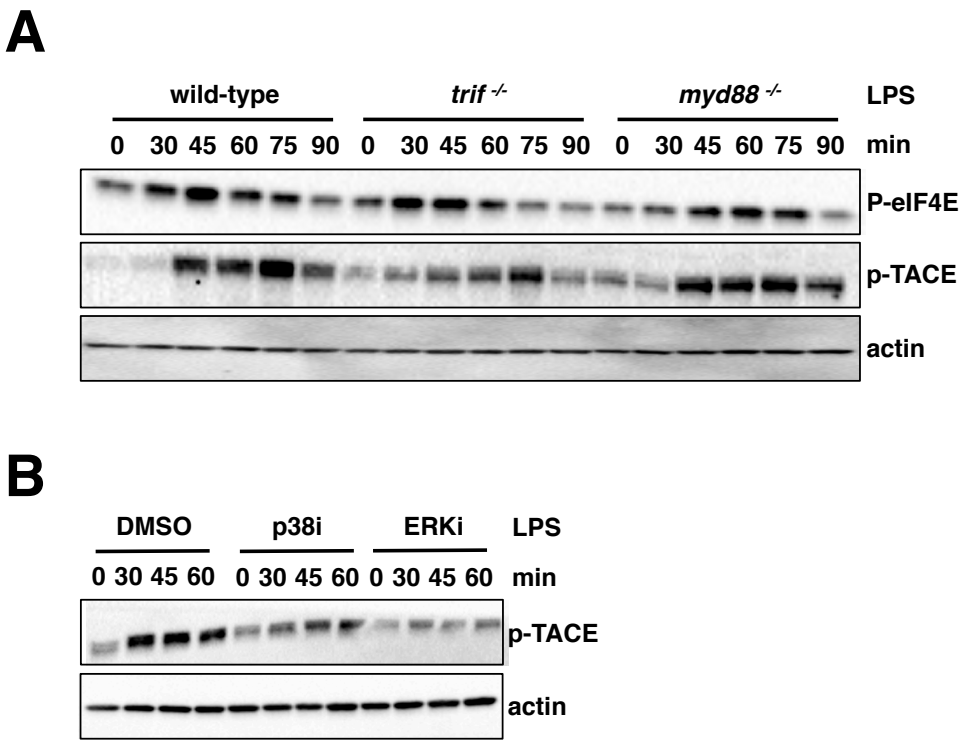

Figure 2.12 TRIF controls eIF4E and TACE activation
A Immunoblot for phospho-eIF4E, phopsho-TACE, and actin in wild-type, *trif* $^{-/-}$, and *myd88*$^{-/-}$ BMDMs stimulated with 10ng/mL. Phospho-eIF4E, n=2; p-TACE, n=3. **B** Immunoblot for phospho-TACE and actin in wild-type BMDMs pre-treated with DMSO, 10μM p38 inhibitor, or 10μM ERK inhibitor for 1 hour followed by stimulation with 10ng/mL LPS. Blot is representative of 2 experiments.

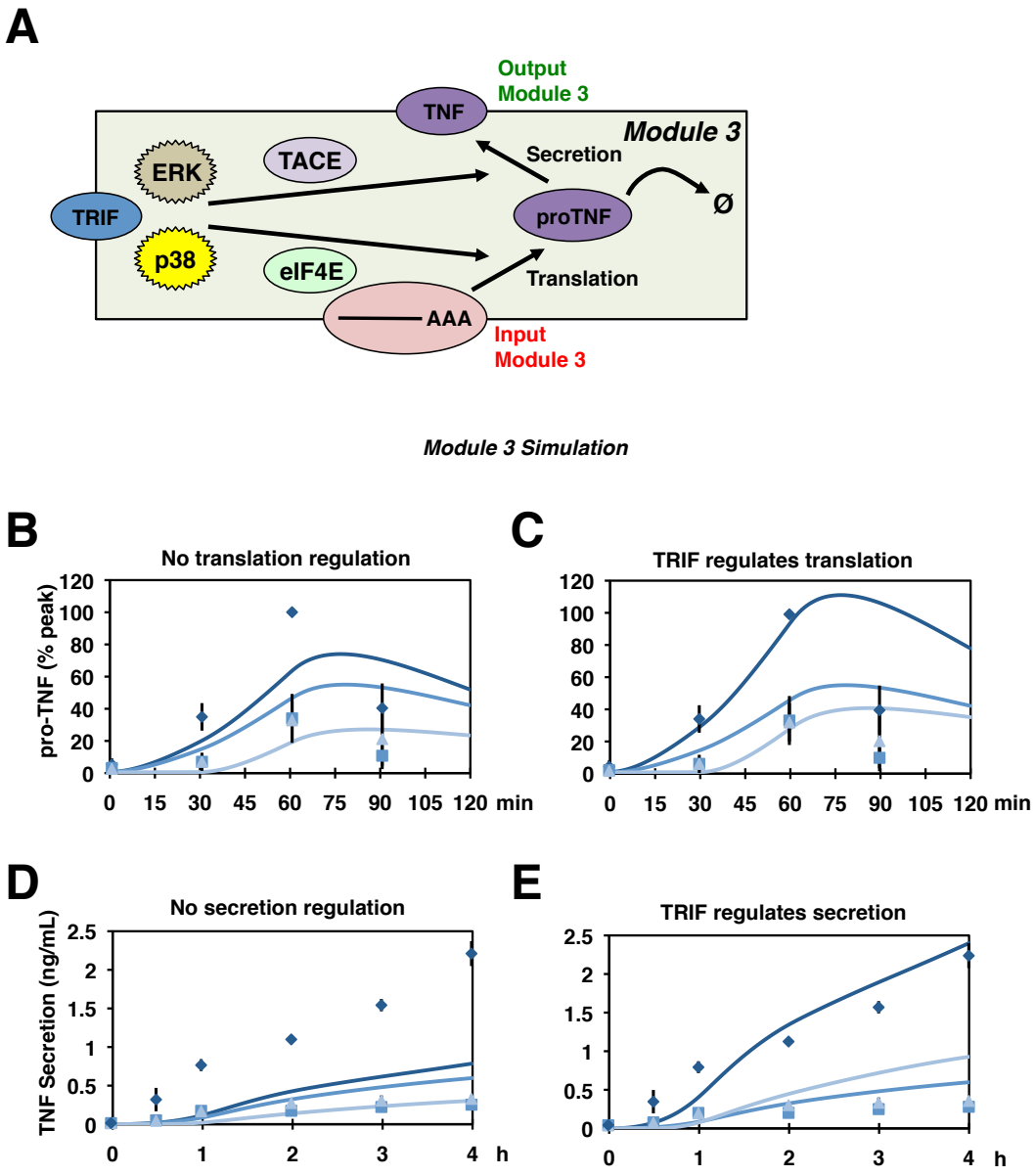

Figure 2.13 A model for TRIF-mediated translation and secretion
A Schematic of module 3 describing the promotion of TNF translation and secretion controlled by TRIF. Input: mature TNF mRNA levels from Module 2 simulations; Output: secreted TNF. **B-E** Lines: simulations of module 3 measure proTNF expression (top) and secreted TNF (bottom) with and without the promotion of TNF procession through TRIF-mediated translation and secretion regulation. Data points: experimental data for pro-TNF expression (top 2 graphs) or TNF secretion (bottom 2 graphs) in wild-type, *trif* $^{-/-}$, or *myd88*$^{-/-}$ BMDMs stimulated with 10ng/mL LPS as reported in 2.10 and 2.1D.

Chapter 3: Network dynamics determine the autocrine and paracrine functions of TNF

Introduction

Computationally modeling inflammatory processes and immune signaling networks presents a considerable challenge: how can mathematical models be created that can recapitulate complex experimental data and make predictions of network dynamics in to alternative stimulus conditions without becoming prohibitively large in scale? Furthermore, modeling a signaling process, such as the production of a cytokine in response to TLR agonists, must be placed in the wider context of the inflammatory signaling network of which it is involved. This systems biology approach of combining experimental studies with computational models to achieve quantitative and qualitative insights has been particularly fruitful in the study of signal transduction (Basak et al., 2012; Ozaki et al., 2005; Purvis and Lahav, 2013).

In chapter 2, we presented the quantification of experimental results to inform modules with simple topologies for key steps in the production of TNF. These individual modules describe the minimal singaling ecents sufficient to explain each step of TNF production, and can be sequentially connected to form a model that recapitulates experimentally observed TNF levels at all steps. We have demonstrated the benefits to using this modular approach to signaling networks previously, publishing models for TNFR-, and TLR-, and NFκB signaling modules (Cheng et al.; Werner et al., 2005, 2008). Thus, we can place our computational characterization of TNF production within the larger context of TLR and TNFR signaling.

The production and secretion of TNF in response to TLR agonists is a dynamic and stimulus-specific process. Once secreted by macrophages, TNF can signal in both autocrine and paracrine manners to modulate the inflammatory process, leading to transcription factor activation, cytokine and chemokine production, microbiocidal pathway activation, and finally attenuation. While the individual roles that TNF carries out in inflammatory signaling have been well studied, there still exists a need for a quantitative understanding of the autocrine and paracrine signaling of TNF within the wider inflammatory signaling network. By constructing a mathematical model of the inflammatory signaling network based on the building block modules previously parameterized and validated using experimental data, we can make predictions of the autocrine and paracrine signaling effects of TNF for a variety of TLR agonists. These unique mathematical predictions can then be tested and validated through experimentation, giving rise to a new, quantitative understanding of the dynamics of TNF signaling.

Materials and Methods

Animals and cell culture

For all experiments using mice, the C57BL/6 strain was used. These mice were housed at the University of California, San Diego (UCSD) in pathogen-free conditions. The experiments performed using mice were in accordance with protocols authorized by the UCSD Institutional Animal Care

and Use Committee. Bone Marrow-Derived Macrophages (BMDMs) were made through the isolation of 6 x 10^6 bone marrow cells from C57BL/6 mouse femur and tibia bones from wild-type, *trif*$^{-/-}$, and *myd88*$^{-/-}$ mice. To differentiate into BMDMs, BM cells were cultured in L929-conditioned media for 7 days in 15cm suspension dishes at 37°C and 5% CO_2. On day 7, the differentiated BMDMs were collected and re-plated in Dulbecco's modified Eagle's medium (DMEM) supplemented with 10% fetal bovine serum at a density of 2 x 10^6 cells per 6cm culture dish.

Analysis of Secreted TNF

For all ELISA experiments to measure the concentration of secreted TNF, BMDMs were replated on day 7 at a density of 2 x 10^6 cells per 6cm culture dish in DMEM supplemented with 10% fetal bovine serum. On day 8, BMDMs were stimulated with 10ng/mL of LPS (Sigma, B5:055), 500nM CpG DNA (Invogen ODN 1668), or PolyI:C in 1mL of DMEM media per plate. After stimulation for each indicated time, the media from each plate was collected and stored at -20°C until processed. To measure the concentration of TNF secreted by BMDMs into the media, ELISAs were performed using the mouse TNF alpha ELISA Ready-SET-Go!® kit in Corning Costar 9018 high affinity binding 96-well plates (affymetrix eBioscience cat #88-7324-77). TNF concentration in cell media was measured in triplicate wells and incubated overnight at 4°C. Standard solutions of 2-fold dilutions of 1000pg/mL mouse

TNF standard down to 7.5pg/mL were used and a standard curve applied as in the manufacturer's guidelines. ELISA 96-well plates were read using a BioTek Epoch Micro-Volume Spectrophotometer System.

RNA extraction and cDNA preparation

For all mature mRNA analysis, BMDMs were replated on day 7 at a density of 2 x 10^6 cells per 6cm culture dish in DMEM supplemented with 10% fetal bovine serum. On day 8, BMDMs were stimulated with 10ng/mL LPS, 500nM CpG, or 50µg/mL PolyI:C in 1mL of DMEM media per plate. For RNA extraction, the plates were washed with ice-cold PBS+1mM EDTA and total RNA was extracted using Qiagen QIAshredder and RNeasy kits according to the manufacturer's guidelines (Qiagen). RNA was eluted with 30µL of RNase-free water and stored at -80°C. cDNA libraries were created from 500ng of total RNA using the Bio-Rad iScript cDNA synthesis kit per the manufacturer's instructions (Bio-Rad).

RT-PCR

In order to measure the mature mRNA expression levels of TNF and the housekeeping gene GAPDH, quantitative real-time PCR (RT-PCR) was used. For mature mRNA expression level analysis, primers for TNF and the housekeeping gene GAPDH were designed (listed in Table 2.1). Samples were analyzed in triplicate in 384 PCR plates using 1.0µl cDNA template, 1.0µl

(100 nM final concentration) of each primer, and 2.5µl SsoAdvanced SYBR Green Supermix (Bio-Rad). qRT-PCR was performed on a Bio-Rad CFX384 Real-Time Detection System and analyzed using the Bio-Rad CFX Manger Software v1.6, with amplification of genes of interested represented in quantifaction cycle (Cq) values. Fold changes (represented on log2 and linear scales) for all time points within experiments are relative to the wild-type 0 timepoint, calculated by the Δ(ΔCq) method previously described (Schmittgen and Livak 2008).

Nuclear extraction and gel shift assays

BMDMs were replated on day 7 at a density of 2 x 10^6 cells per 6cm culture dish in DMEM supplemented with 10% fetal bovine serum. On day 8, BMDMs were stimulated with 10ng/mL of LPS or 100nM CpG in 1mL of DMEM media per plate. CE Buffer (10mM HEPES pH 7.9, 10mM KCl, 0.1mM EGTA, 0.1mM EDTA, 1mM DTT, 1mM PMSF, 10µg/ml aprotinin and 5µg/ml leupeptin) was added to plates to collect cells. 0.5% NP-40 was then added to each sample and vortexed. Nuclei pellets were formed by centrifugation at 4000g for 1 minute, followed by resuspension of nuclei pellets in 15µL of nuclear extract buffer (20 mM HEPES ph 7.9, 400mM NaCl, 1.5mM $MgCl_2$, 0.2mM EDTA, 25% glycerol, 1mM DTT, 1mM PMSF, 10µg/ml aprotinin and 5µg/ml leupeptin). The nuclear lysates were centrifuged at 14,000g at 4°C for 5 minutes, and protein concentrations determined by Bradford assay (Bio-

Rad). Nuclear lysates from each experiment were normalized, and Electrophoretic Mobility Shift Assays (EMSAs) performed as described previously (Werner et al. 2005). Nuclear lysates were incubated at room temperature for 15 minutes with a P^{32}-labelled HIV G1G2 probe, a double-stranded oligonucleotide that contains two κB sites: (GCTACAAGGGACTTTCCGCTGGGGACTTTCCAGGGAGG). Samples were applied to and run on a non-denaturing acrylamide gel to separate bands corresponding to activated NFκB binding the κB-containing P^{32}-labelled probe. These bands were captured by audioradiography and analyzed using software (GE). Quantification of bands was performed by measuring the absolute intensity of each p65-p50 NFκB dimer band and normalizing all intensities to peak wild-type band intensity.

Immunofluorescence imaging of co-cultured 3T3s and BMDMs

3T3s used in all imaging and co-culturing experiments were *trif*$^{-/-}$*myd88*$^{-/-}$ 3T3s grown in DMEM supplemented with 10% bovine calf serum. On day 7 of culturing in L929-condition growth media, BMDMs isolated from *tnfr*$^{-/-}$ mice were collected and labeled using Cell Tracker™ Red CMTPX (Life Technologies C34552). Labeled BMDMs were subsequently co-cultured with *trif*$^{-/-}$*myd88*$^{-/-}$ 3T3s in Corning 24-well plates, containing glass slides (Fisher), in DMEM supplemented with 10% bovine calf serum, at a ratio of 2.5:97.5 ratio. For control experiments, *trif*$^{-/-}$*myd88*$^{-/-}$ 3T3s alone were stimulated with

10ng/mL TNF, 1μg/mL LPS, or 1μM CpG for 15 minutes (TNF) or 75 minutes (LPS, CpG). On day 8, co-cultures of BMDMs and *trif*$^{-/-}$*myd88*$^{-/-}$ 3T3s were stimulated with 1μg/mL LPS or 1μM CpG for 75 minutes. The slides in the plates were washed twice with PBS and then fixed using 4% paraformaldahyde (EM Sciences) in PBS for 15 minutes at room temperature. Slides were then washed again twice with PBS. Slides were blocked with 5% Normal Goat Serum, 0.2% Triton-X100 in PBS and stained with p65 (Santa Cruz Rabbit sc-372) primary antibody in blocking buffer at 1:200 dilution overnight at 4°C. Secondary antibody goat-anti-rabbit Alexafluor-488 (Life Technologies) was used at a dilution of 1:1000, and incubated at room temperature for 1 hour. Nuclei were counterstained with Hoechst and images were acquired on an Axio Observer Z1 inverted microscope (Carl Zeiss Microscopy GmbH, Germany) with a 20x, 1.3 NA oil immersion objective to a Coolsnap HQ2 CCD camera (Photometrics, Canada) using ZEN imaging software (Carl Zeiss Microscopy GmbH, Germany). Cell nuclei were manually counted and scored for nuclear translocation of NFκB subunit p65.

RNA-Seq

For RNA-Seq experiments, BMDMs were replated on day 7 at a density of 2 x 10^6 cells per 6cm culture dish in DMEM supplemented with 10% fetal bovine serum. On day 8, BMDMs were stimulated with 100nM or 500nM CpG in 1mL of DMEM media per plate. For RNA extraction, the plates were washed

with ice-cold PBS+1mM EDTA and total RNA was extracted using Qiagen QIAshredder and RNeasy kits according to the manufacturer's guidelines (Qiagen). RNA was eluted with 30μL of RNase-free water and stored at -80°C. cDNA libraries were prepared for RNA-Seq using the TruSeq Stranded mRNA HT Kit according to the manufacturer's instructions (illumina ref #15032623). Quantitation was performed using the Roche Light Cycler 480. Sequencing was performed on Illumina's HiSeq 2000, according to manufacturer's recommendations and prepared for RNA sequencing analysis by the BSCRC High Throughput Sequencing Core at the University of California, Los Angeles. Reads were aligned to the ENSEMBL NCBI m37 mouse genome build, release 66 (Flicek et al., 2012) with the STAR RNA seq aligner (Dobin et al., 2013). HTSeq-count from the HTSeq python package (Anders et al., 2014) was used to determine raw gene read counts. The total number of reads mapping to features in each sample was used to normalize to counts per million (cpm). Genes not induced or with less than 10 cpm in all low dose wild-type conditions were removed from consideration. After a 25cpm pseudo count was added to all of the genes, the $\log_2$ was taken for every condition. The log fold change for each timepoint and gene are relative to the wild-type 0-hr timepoint. For k-means clustering, the timepoints each gene were divided by the respective genes's maximum expression level.

Computational Simulations

This TNF production model detailed in Chapter 2 was connected with a model for TLR-induced IKK activation (Cheng et al.) and IKK-induced NFκB activation (Hoffmann et al., 2002; Werner et al., 2005) to produce a mult-modular. Iterative simulation and experimentation led to the inclusion of the TNFR model (Werner et al., 2008) to allow for autocrine TNF signaling. Simple As in Chapter 2, the multi-modular model conists of Ordinary Differential Equations (ODEs) from the receptor engagement of ligand to the production of TNF and subsequent autocrine signaling through TNFR. The fitness of each mathematical model to math experimental data was determined and scored by RMSD. MATLAB version R2013a (The MathWorks Inc.) was used to numerically solve ODEs with the subroutine *ode15s.*

A mathematical model of TLR agonist-responsive TNF production

To characterize TLR-induced TNF production, we connected our three models for each step in TNF production with the model for TLR-induced IKK activation coordinated through MyD88 and TRIF activities, and the model for IKK-induced NFκB activation, creating one model that computationally characterizes TLR agonist-induced TNF production (Figure 3.1) (Cheng et al.; Werner et al., 2005). Computationally simulating LPS-induced TNF production in the wild-type condition demonstrates that the mathematical model is able to recapitulate the experimental data at the level of nascent RNA, mature mRNA,

pro-TNF production, and TNF secretion (Figure 3.2). Expanding the computational simulations to the *trif*$^{-/-}$ and *myd88*$^{-/-}$ conditions, however, reveals that while the model is able to capture TRIF dynamics (in the *myd88*$^{-/-}$), it is not able to accurately capture MyD88 dynamics, particularly at the level of nascent RNA and mRNA production (Figure 3.3). To investigate these adaptor-specific differences further, we then used the model to predict the TNF production dynamics of two other TLR agonists, PolyI:C (TLR3/TRIF agonist) and CpG DNA (TLR9/MyD88 agonist). Here, the model was able to successfully predict PolyI:C-induced TNF production at the level of mRNA and protein secretion (Figure 3.4). However, the present form of the model was not able to recapitulate CpG-induced dynamics of TNF mRNA production or secretion. Given the previous reports on the ability of TNF to signal in an autocrine manner, we posited that perhaps autocrine TNF in response to CpG led to the persistence of TNF mRNA and protein secretion, so we sought to investigate this further.

The autocrine signaling function of TNF augments NFκB activation in response to CpG.

Incorporating these three modules into one signaling network in a straightforward, stepwise fashion allows us to characterize the temporal dynamics of TNF production. Previous reports suggest that TNF may signal in an autocrine fashion and play a role in augmenting NFκB activation in

response to certain stimuli conditions. The nature of the TNF model, with various TLR-agonist inputs that induce different adaptor-mediated kinetics, gives us the ability to investigate the potential autocrine function of TNF and make predictions that can be tested experimentally. Therefore, we expanded the mathematical model to include autocrine TNF signaling by incorporating the module for TNFR-mediated NFκB activation (Werner et al., 2008) (Figure 3.5). We then simulated the multi-modular model for LPS, CpG, and PolyI:C stimulation conditions to determine whether autocrine feedback in the model would allow for a better prediction of experimental data. Here, we found that autocrine TNF signaling had little effect on TNF production levels in the LPS and PolyI:C stimulated conditions, but drastically improved the ability of the model to predict CpG-induced TNF mRNA production and protein secretion (Figure 3.6). To determine whether this prolonging of CpG-induced dynamics was due to persistent NFκB activity induced by autocrine TNF, we simulated the model for NFκB activation with and without TNF autocrine feedback. In this scenario, the model predicts that while LPS-induced NFκB will not be affected by the loss of autocrine TNF, CpG-induced autocrine TNF is required for persistent NFκB activity (Figure 3.7A). To test this experimentally, NFκB activity was measured in the absence of TNF autocrine signaling using *tnf*$^{-/-}$ mice, which are deficient in TNF production. Wild-type and *tnf*$^{-/-}$ BMDMs were stimulated with either LPS or CpG followed by EMSAs for NFκB activation. These results confirmed the computational prediction, demonstrating that

while *tnf*$^{-/-}$ BMDMs did not have reduced NFκB activation in response to LPS, they did have reduced NFκB activation in response to CpG from 4-8 hours (Fig 3.7B). This aligns with the result from the model, which predicted that stimuli that signal transiently, such as a CpG mediated through MyD88, would be more dependent on TNF autocrine feedback for late NFκB activation. This result suggests that in response to CpG, secreted TNF serves an essential autocrine role.

TLR-agonist induced kinetics of TNF production encodes autocrine and paracrine functions

Computational simulations of the multi-modular model led to the prediction that sustained NFκB activity in response to CpG would be dependent on CpG-induced TNF autocrine signaling, which was confirmed by experiments in *tnf*$^{-/-}$ BMDMs. As NFκB is a transcription factor that controls many inflammatory genes, we next sought to determine the role that CpG-induced autocrine TNF signaling plays at the level of gene transcription. To do this, wild-type and *tnf*$^{-/-}$ BMDMs were stimulated with CpG up to 24 hours, and RNA-seq was performed on collected extracts. Analysis of RNA-seq data revealed that 267 genes were significantly upregulated by CpG stimulation (Figure 3.8). K-means clustering identified clusters of genes that showed either a strong early peak induction (cluster E), a peak at 8 hours but persistent induction (cluster B and F), a peak at 8 hours followed by a

decrease by 24 hours (clusters A and D), or a slow induction resulting in a peak at 24 hours of stimulation (cluster C). We examined a few genes specifically whose expression was partially dependent on TNF (Fig 3.9). These included genes involved in bacterial recognition and killing (Clec4e, Ascl1, Gbp6), inflammasome activation (nod2, Mefv, Ifi205), macrophage resolution (Tmem178, Fzd1, Hp), NFκB attenuation (NFκB ie, Mlt1, Tnfaip3), and adaptive immune control (tnfsf15, Fam26f, Slamf8). Not surprisingly, numerous of these highlighted gene are known to be controlled by NFκB, demonstrating that TNF autocrine signaling not only has a general effect on prolonging the inflammatory state, but that the observed decrease in NFκB activity seen in *tnf*$^{-/-}$ BMDMs stimulated with CpG leads to a phenotype of decreased NFκB-dependent gene expression.

Next, we sought to investigate the paracrine role that secreted TNF serves in response to LPS and CpG. Tissue-resident macrophages exist in an environment where they secret cytokines and signal to other cell types in the tissue, such as fibroblasts, which respond and are activated by the macrophages signals. To construct an experimental system that mimics this tissue-resident macrophage environment, BMDMs generated from *tnfr*$^{-/-}$ mice were co-cultured with *myd88*$^{-/-}$ *trif*$^{-/-}$ 3T3s, which cannot activate NFκB in response to TLR signaling. In this setup, the initial stimulus (LPS or CpG) activates the *tnfr*$^{-/-}$ BMDMs, but not the *myd88*$^{-/-}$ *trif*$^{-/-}$ 3T3s. However, the TNF secreted by the *tnfr*$^{-/-}$ BMDMs is able to activate the *myd88*$^{-/-}$ *trif*$^{-/-}$ 3T3s, which

is measured by immunofluorescent staining for NFκB subunit p65 (Fig 3.10A). This microscopy experiment reveals that LPS-induced TNF secretion plays a strong paracrine role, as more *myd88*$^{-/-}$ *trif*$^{-/-}$ 3T3s near TNF-secreting BMDMs show significant p65 nuclear translocation (Fig 3.10B). However, in the CpG-stimulated condition, *myd88*$^{-/-}$ *trif*$^{-/-}$ 3T3s showed less p65 translocation the LPS-stimulated condition. These results lead us to conclude that LPS-induced TNF secretion plays a primarily paracrine role, while CpG-induced TNF secretion plays an autocrine role in NFκB activation.

Discussion

Previously, our lab has published mathematical models based on modules for TNFR-mediated IKK activation and IKK-mediated NFκB activation (Hoffmann et al., 2002; Werner et al., 2005, 2008). In chapter 2, we determined topology for three modules describing steps in the production and regulation of TNF, and used experimental rates to parameterize mathematical models based on these modules. However, the utility of models based on signaling modules are limited unless they can be used as building blocks for larger signaling networks. To this end, in this chapter we have combined the three TNF modules together with the previously published modules for TLR-mediated IKK activation, TNFR-mediated IKK activation, and IKK-mediated NFκB activation to construct one stimulus-specific predictive module for TNF production. By iteratively performing this dual experimental and computational

approach, and characterizing each single stage of TNF production, we are able to test the sufficiency of the network architecture by simulating the module for different stimuli and make predictions about the signaling functions of TNF within the network.

The experimental approach revealed LPS stimulation of macrophages confers a strong, early, and persistent TNF secretion through the combination of fast MyD88-mediated NFκB activation leading to RNA transcription and later TRIF-mediated promotion of TNF processing. In contrast, while CpG induces significant NFκB activation and TNF RNA transcription rapidly, TNF secretion takes longer to reach LPS-stimulated levels due to the lack of TRIF-induced promotion of TNF processing, as TLR9 does not use TRIF as an adaptor. While the first iteration of the computational TNF module was able recapitulate LPS-stimulated TNF secretion dynamics, it was not able to recapitulate CpG-stimulated dynamics. This led us to incorporate this TNF production module to the previously published modules for TNFR signaling, creating a single model for NFκB activation, TNF production, and TNF feedback in TLR-induced signaling in order to account for the differential dynamics of stimulus-specific NFκB activation and TNF production. By including autocrine TNF signaling into the mathematical model, we were able to capture the dynamics of TNF secretion seen experimentally for CpG stimulation. Furthermore, a benefit of this iterative approach also led us to suspect that sustained TLR-induced NFκB activation may be dependent on autocrine TNF, a phenomenon that the

model indeed predicted through simulation for CpG, but not for LPS. Testing this experimentally revealed that CpG-induced sustained NFκB activity is indeed dependent on autocrine TNF, demonstrating the robustness and predictive ability of the model.

Upon confirming through experimental and computational approaches that CpG-induced TNF signals in an autocrine manner to sustain NFκB activity, we then decided to investigate the functional consquenences of autocrine TNF signaling. To do this, we performed RNA-Seq in CpG stimulated wild-type and *tnf* $^{-/-}$ BMDMs, the latter condition removing the possibility of autocrine TNF signaling. Here, 267 upregulated genes were clustered into 6 clusters. GO analysis revealed that the first two clusters that showed a significant decrease in the *tnf* $^{-/-}$ condition were ranked very highly for inflammatory cytokine production, which is strongly influenced by TNF signaling. Characterization of genes with significantly decreased induction in the *tnf*$^{-/-}$ condition revealed numerous NFκB-controlled genes and demonstrated that TNF induces the expression of genes critically related to inflammatory macrophage function, at the level bacterial recognition and killing, inflammasome activation, NFκB attenuation, macrophage resolution, and adaptive immune control. These genes highlight the pleitropic role that autocrine TNF signaling plays in macrophage inflammation.

Surprisingly, LPS-induced autocrine TNF did not have an effect on NFκB activation. This led us to surmise that LPS-induced TNF may have a

stronger role as a paracrine signaler. To test this, we co-cultured *tnfr* $^{-/-}$ BMDMs with *trif*$^{-/-}$*myd88*$^{-/-}$ 3T3s and stimulated with either LPS or CpG. The *trif*$^{-/-}$*myd88*$^{-/-}$ 3T3s served as sensors for the paracrine TNF secreted by the stimulated BMDMs, where NFκB subunity p65 nuclear translocation was used to correlate the strength of paracrine signaling that the two TLR agonists induced. This experiment revealed that LPS-induced TNF plays a much stronger paracrine-signaling role than CpG-induced TNF.

In summary, in Chapter 3 we constructed a model for TNF production and signaling functions in the context of TLR agonist-induced inflammatory signaling. Furthermore, we used this model to make predictions about the stimulus-specific functions of TNF autocrine and paracrine signaling, leading to the revelation that CpG-induced TNF signals in a primarily autocrine manner, while LPS-induced TNF signals in a primarily paracrine manner.

Acknowledgements

Chapter 3, is a modified presentation of material that is being prepared for publication as “Network dynamics determine the autocrine and paracrine signaling functions of TNF” by Caldwell AB, Cheng Z, Vargas J, Birnbaum H, and Hoffmann A. The dissertation author was the primary investigator and author of this material. Zhang Cheng performed the mathematical modeling and computational simulations. Jesse Vargas performed immunofluorescence microscopy imaging and analysis of immunofluorescence data. Harry Birnbaum performed the analysis of the RNA-Seq data. Kim Ngo provided assistance with the creation of RNA-Seq libraries.

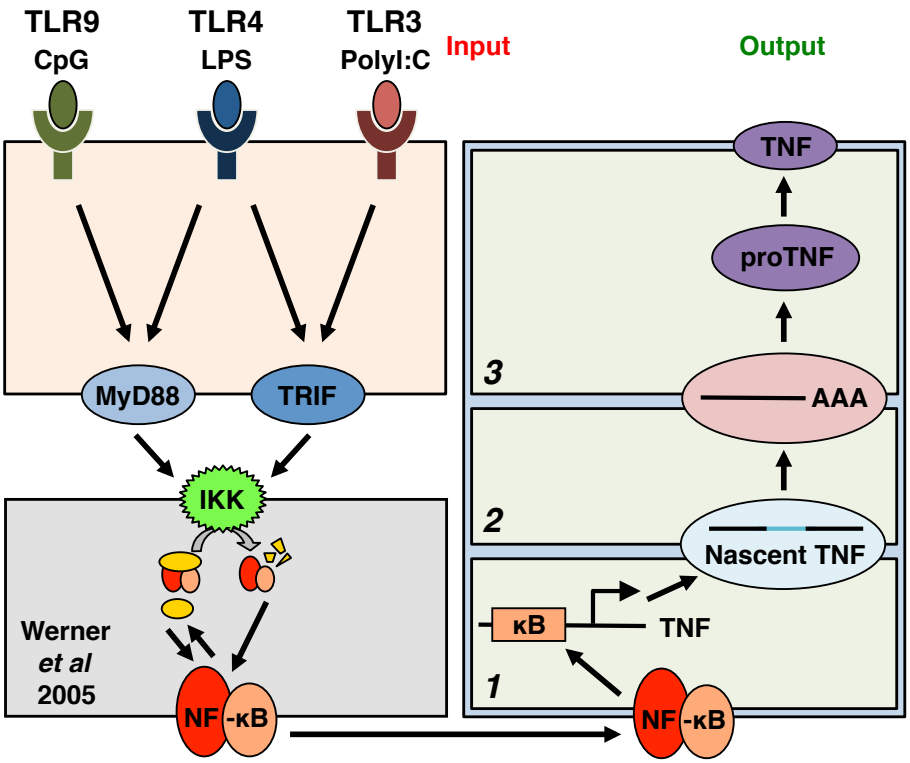

Figure 3.1 The multi-modular mathematical model for TNF production
A Schematic of the computational model combining modules for TLR receptor activation to adaptors TRIF and MyD88, activation of IKK and NFκB, and the 3 modules for TNF production.

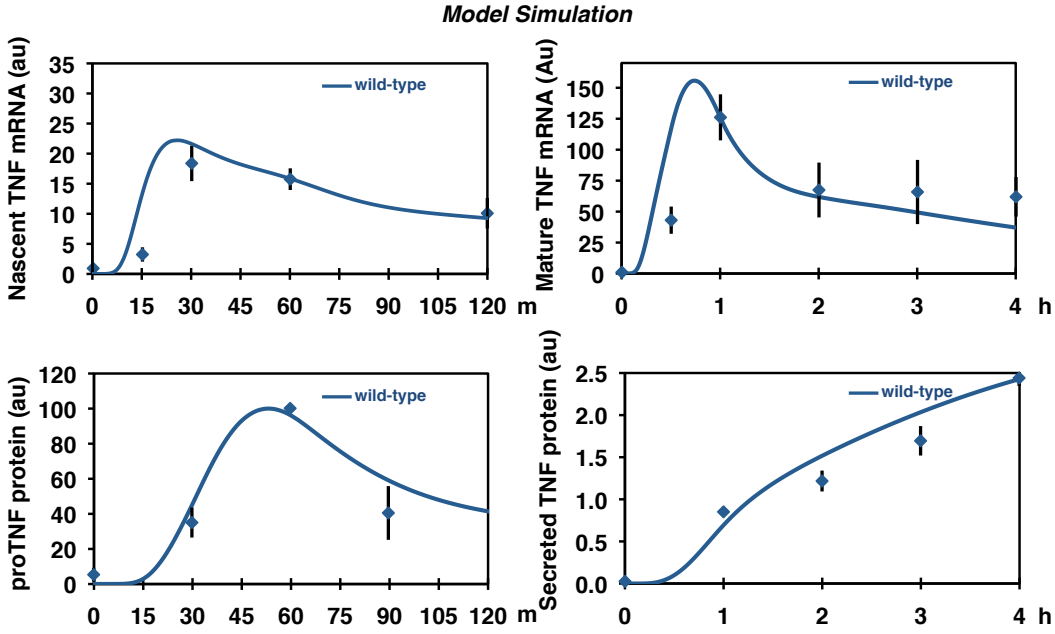

Figure 3.2 The multi-modular model accounts for LPS-mediated TNF production in wild-type cells

Model simulations and experimental data for wild-type cells in response to 10ng/mL LPS; solid lines indicate values of model simulations, data points represent experimental data represented in previous figures.

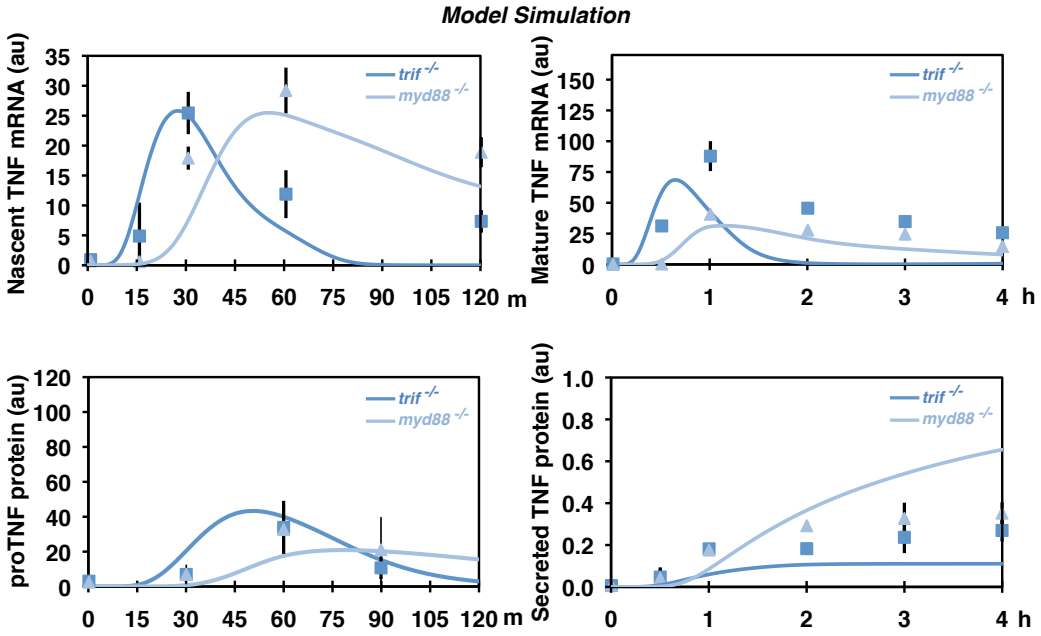

Figure 3.3 The multi-modular model accounts for LPS-mediated TNF production in MyD88-deficient cells but not TRIF deficient cells
Model simulations and experimental data, represented as in Figure 3.2, for *trif* $^{-/-}$ and *myd88* $^{-/-}$ cells in response to 10ng/mL LPS.

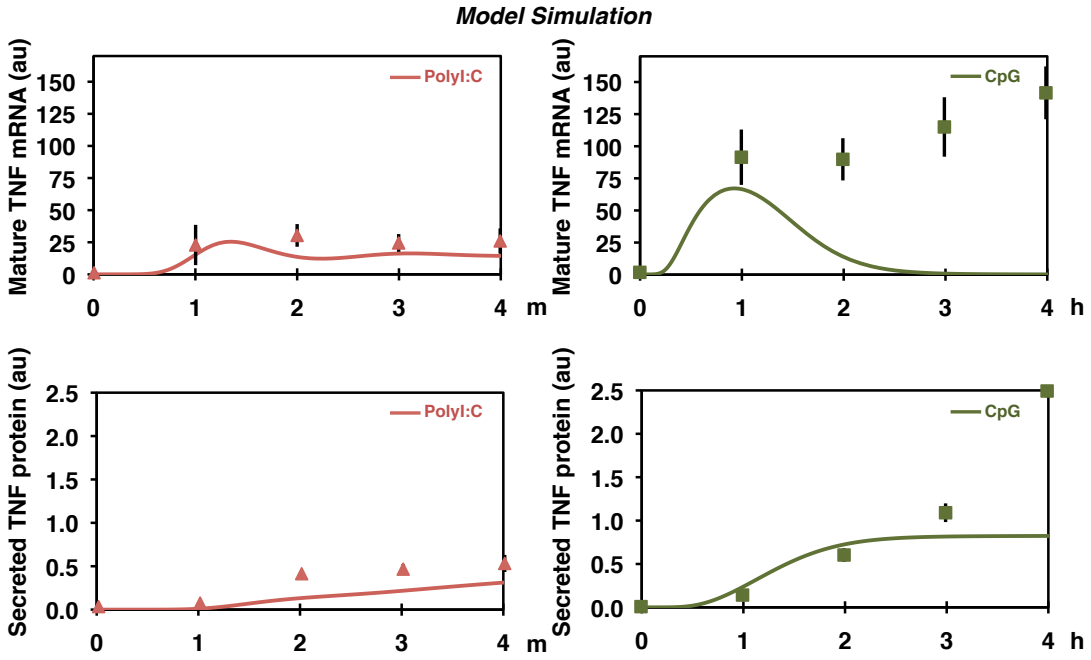

Figure 3.4 The multi-modular model accounts for PolyI:C-mediated TNF production but not CpG-mediated TNF production
Model simulations and experimental data for mature TNF mRNA and secreted TNF, represented as in Figure 3.2, for wild-type cells in response to 500nM CpG and 50µg/mL PolyI:C. Error bars indicate one standard deviation from the mean of 3 experiments.

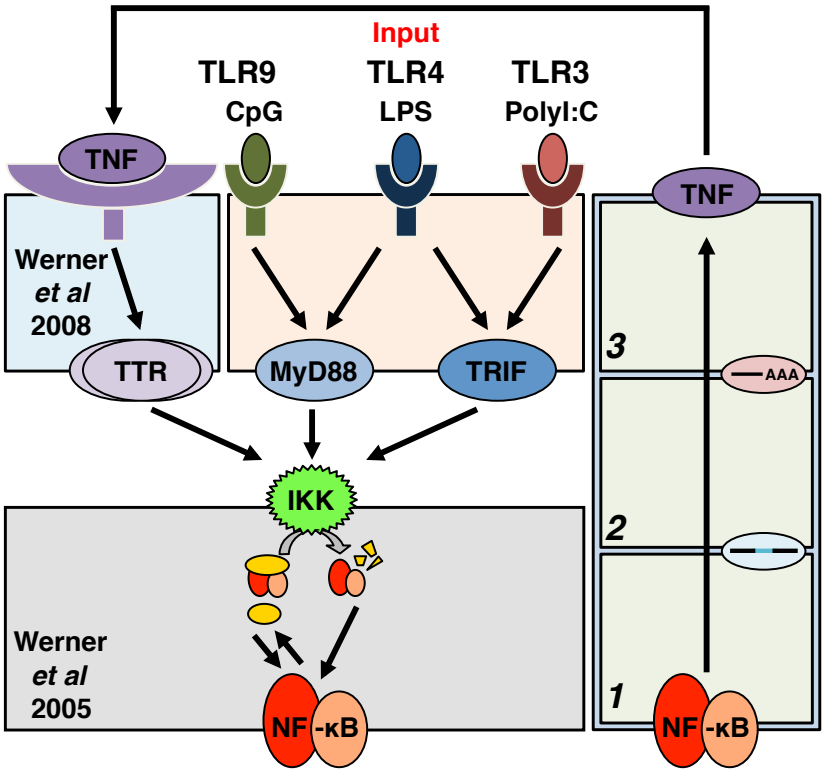

Figure 3.5 Iterative modification of the multi-modular model leads to TNFR module inclusion
Expanded schematic of the computational model in Figure 3.1, incorporating TNF autocrine feedback into NFκB.

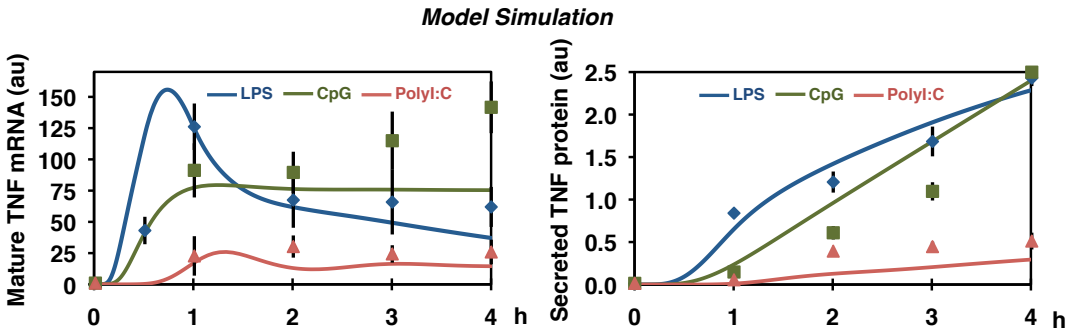

Figure 3.6 The multi-modular model with TNF autocrine feedback can predict CpG-induced TNF production

Model simulations and experimental data for mature TNF mRNA and secreted TNF in wild-type cells stimulated with 10ng/mL LPS, 500nM CpG, or 50µg/mL PolyI:C; solid lines indicate values of model simulations, points represent experimental data represented in previous figures.

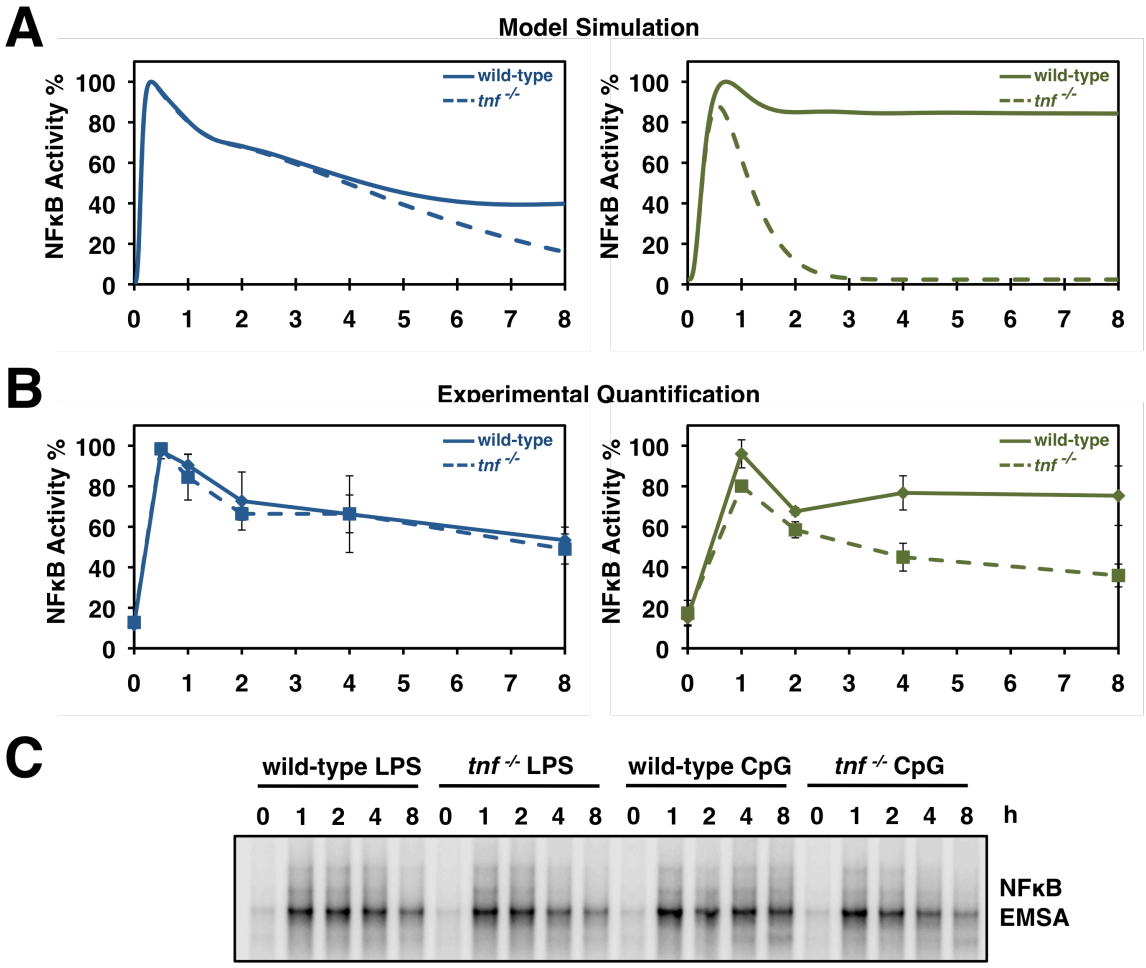

Figure 3.7 TLR-responsive TNF production functions in an autocrine manner in response to some TLR ligands but not others.
A Model simulations for NFκB activity in wild-type or *tnf*$^{-/-}$ stimulated by 10ng/mL LPS or 100nM CpG. Solid lines indicate wild-type simulation, dashed lines indicate *tnf*$^{-/-}$. **B** Experimental validation of model simulations in A. **C** Activation of NFκB measured by EMSA (G1G2 κB-containing HIV probe) in wild-type and *tnf*$^{-/-}$ BMDMs stimulated with 10ng/mL LPS or 100nM CpG. Graphs are quantification of experimental data shown below, normalized to peak wild-type NFκB activation. Gel and quantification is representative of 4 experiments.

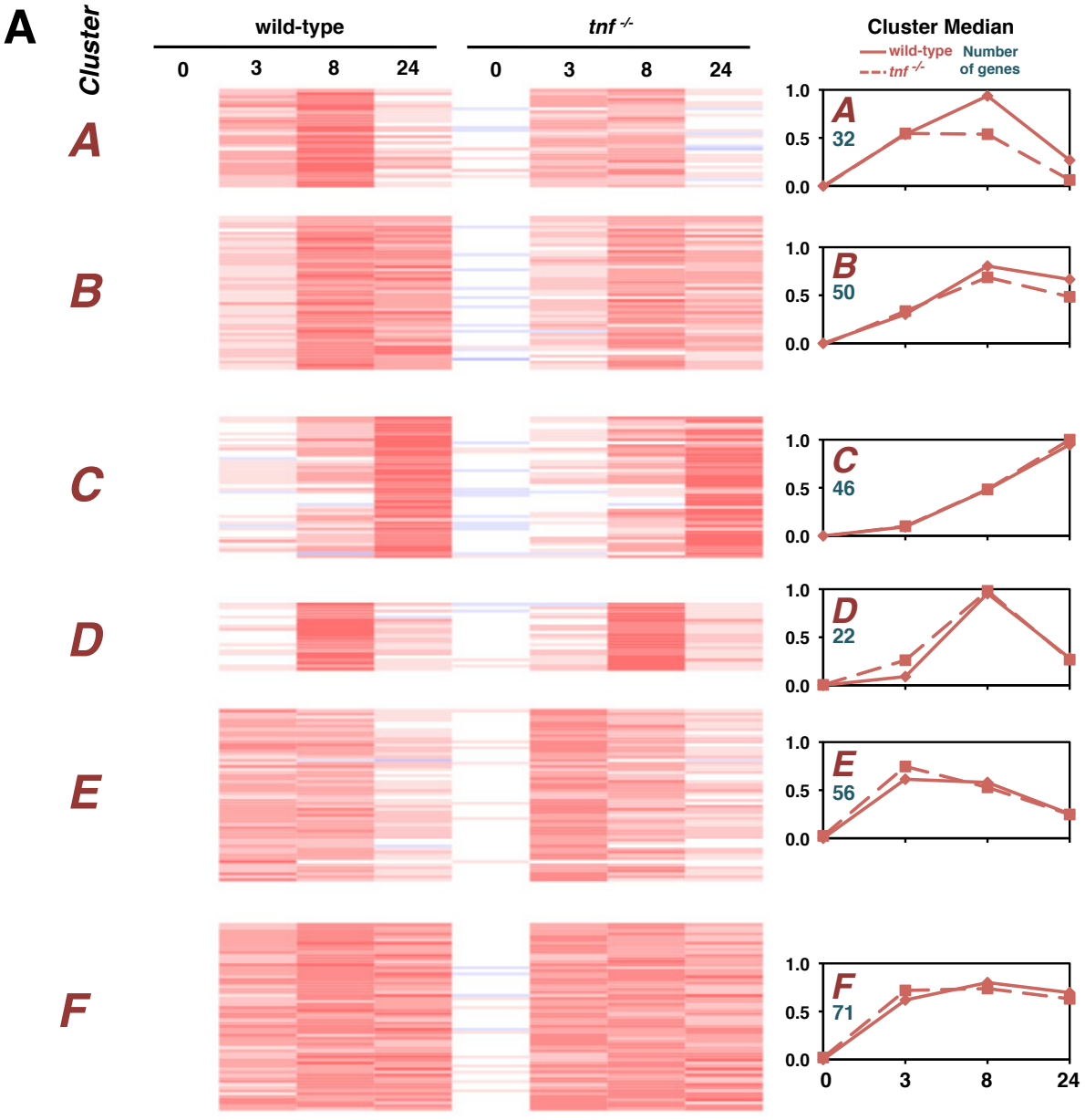

Figure 3.8 Transcriptome analysis reveals autocrine TNF-dependency in certain genes

A RNA-seq data from wild-type and *tnf*$^{-/-}$ BMDMs stimulated with 100nM CpG. K-means clustering led to 6 clusters. Cluster median for each cluster represents the data where the peak RNA induction has been normalized to 1, and the median for each genotype graphed.

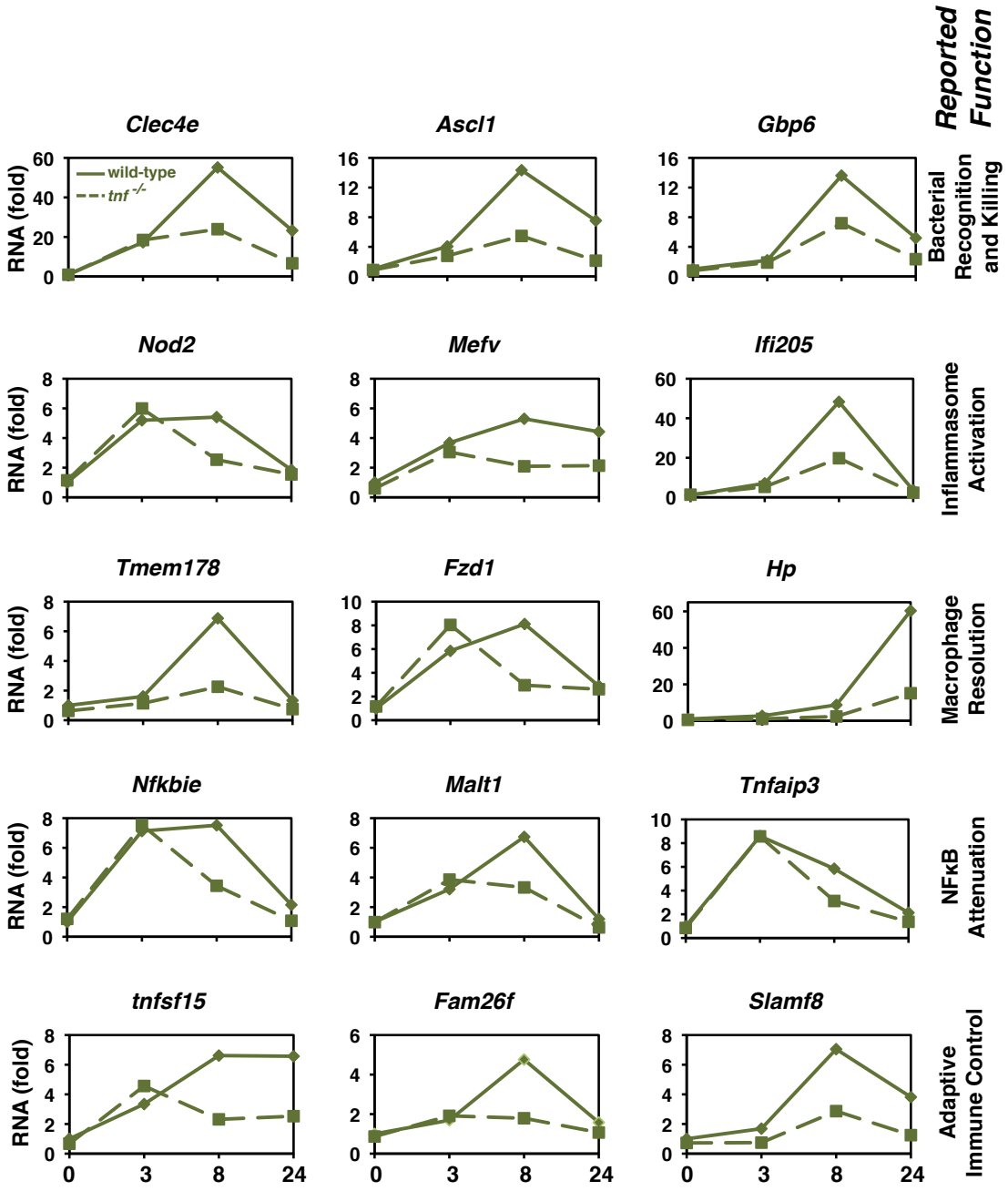

Figure 3.9 CpG-induced autocrine TNF modulates inflammatory gene programs

A RNA-seq data from wild-type and *tnf*$^{-/-}$ BMDMs stimulated with 100nM CpG. Selected genes from the 267 genes upreulated by CpG highlighted and sorted based on reported macrophage function.

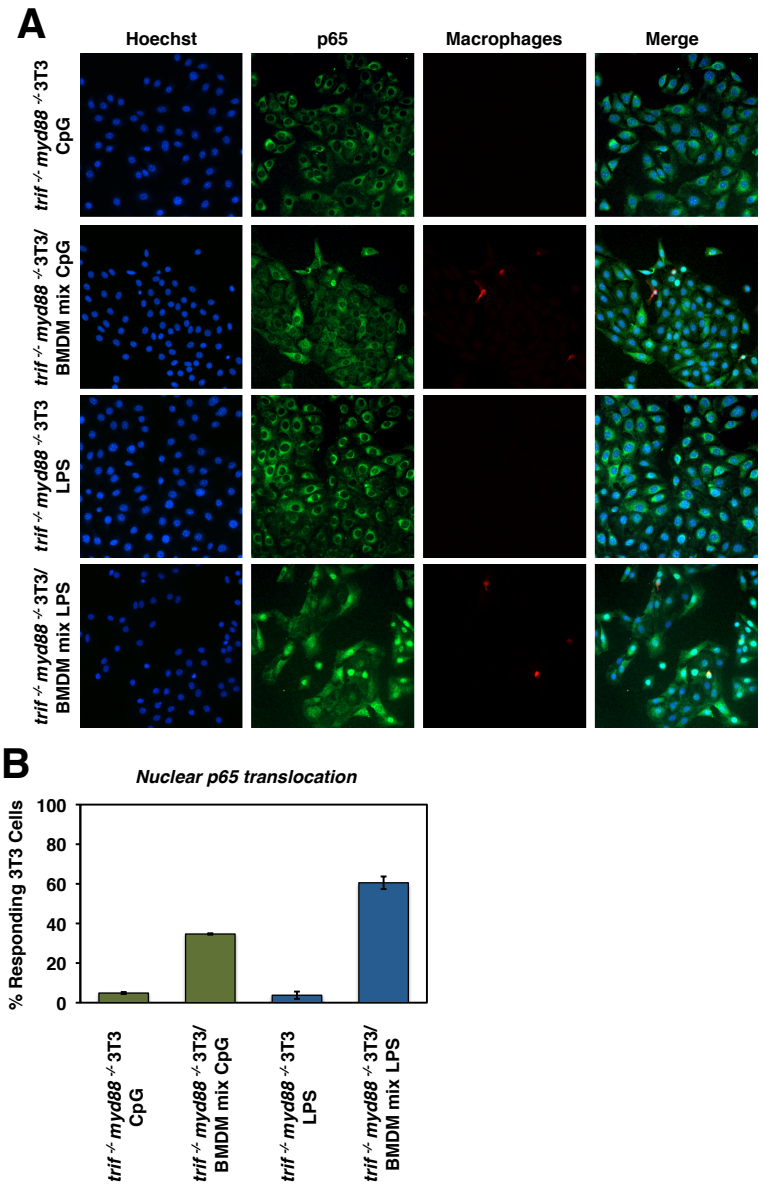

Figure 3.10 LPS-induced TNF signals in a primarily paracrine manner
A Co-culturing of *tnfr*$^{-/-}$ BMDMs with *trif*$^{-/-}$*myd88*$^{-/-}$ 3T3s. First panel, p65-staining of 3T3s stimulated with 1μg/mL LPS for 75 min. Second panel, co-culture of BMDMs with 3T3s stimulated with 1μg/mL LPS for 75 min and stained for p65. Third panel, p65-staining of 3T3s stimulated with 1μM CpG for 75 min. Fourth panel, co-culture of BMDMs with 3T3s stimulated with 1μg/mL LPS for 75 min and stained for p65. Images representative of 4 separate experiments. **B** Bar graphs showing the average number of cells with nuclear p65 in a given field of view, 20-30 images for each experiment. Error bars indicate 1 standard deviation from the mean, n=4.

Chapter 4: Concluding Discussion and Future Direction

In this thesis work, we demonstrate that the network dynamics encoded by specific TLR agonists determine the temporal kinetics of TNF production and its subsequent autocrine and paracrine signaling effects. Surprisingly, we found that while CpG-induced TNF can signal in an autocrine manner, LPS-induced TNF does not have a significant autocrine signaling function in macrophages. Given that the potential autocrine functions of TNF have been suggested to play a role in the inflammatory and innate immune signaling network dynamics downstream of pathogen challenge, this gives rise to the question: why does LPS-induced TNF not signal in an autocrine manner? The answer to this lays in the different receptors that LPS and CpG engage, the adaptors these receptors use, and the resulting temporal kinetics of kinase and transcription factor activation.

LPS engages the TLR4 receptor on the membrane surface of the macrophage cell, where it quickly leads to the recruitment of MyD88 and activation of its pathway downstream. Subsequently, the engaged TLR4 is trafficked to endosomes within the cytoplasm, where TLR4 can recruit TRIF and bring about its pathway activation. EMSAs for NFκB activity in response to LPS in Chapter 2 demonstrated that MyD88-mediated NFκB activation is fast, strong, and transient; in contrast, TRIF-mediated NFκB activation is slower, but significantly more persistent, with activity above basal for at least as long as 4 hours. In addition to NFκB activation, we showed that the LPS-induced TRIF pathway is responsible for accelerating TNF secretion through the

stabilization of TNF mRNA half-life, promotion of pro-TNF translation, and activation of the TACE enzyme that cleaves pro-TNF from the plasma membrane. As a result, LPS-induced TNF secretion occurs in a fast and strong manner, due to the strong gene transcription induced by the MyD88 pathway and the promotion of TNF processing brought about by the TRIF pathway. Autocrine signaling of TNF could be possible as early as 1 hour after stimulation. However, within the 1-2 hour time frame of significant LPS-induced TNF secretion, NFκB activity is still significantly above basal levels due to the TRIF pathway. As a result, the secreted TNF that likely does signal in an autocrine fashion does not lead to further NFκB activity, possibly due to the fact that LPS and TNF induce the activation of similar pools of NFκB (Werner et al., 2008). Furthermore, autocrine TNF engagement of the TNF receptor within 1-2 hours of LPS stimulation likely leads to its internalization, which has been well-reported (Schneider-Brachert et al., 2004). Consequently, although LPS-induced TNF secretion still substantially increases at 3-4 hours, the levels of TNFR on the cell surface may have decreased such that the newly secreted TNF has a lower propensity to signal in an autocrine manner even as TRIF-mediated NFκB activity has decreased.

In contrast, CpG induces the faster MyD88 pathway but not the persistent TRIF pathway. Therefore, while TNF gene transcription occurs quickly and strongly, the lack of the promotion of TNF processing by the TRIF pathway induced by TLR9 results in the slower secretion of TNF. MyD88-

mediated NFκB activation dynamics are more transient, meaning that when CpG-induced TNF secretion reaches a level where it can signal significantly in an autocrine manner, there is likely a larger pool of activatible NFκB than in the LPS stimulated condition. Further, as CpG-induced TNF secretion is slower, there is likely more TNFR on the responding cell's surface able to bind TNF due to less early internalization of the receptor. The delayed production of TNF interfaces with a transient NFκB activity profile triggered by the MyD88 pathway, thus allowing for a potent autocrine feedback effect. The timeframe within which CpG-induced TNF can signal in an autocrine fashion is therefore a consequence of the adaptors that TLR9 uses and the network dynamics that those adaptors elicit. In summary, LPS-induced TNF signals in a more paracrine manner, while CpG-induced TNF signals in a predominately autocrine manner due to differential pathway activation by each respective receptor.

These thesis work highlight the fact that prolonged NFκB activation has evolved to be dependent on secreted cytokine in response to some TLR agonists, while it is hardwired in response to others. Although both LPS and CpG are recognized by overlapping components of the inflammatory and innate immune signaling network, they are disparate pathogen signals. Lipopolysaccharides are large molecules that are integral structures of gram-negative bacteria, and are recognized by TLR4 on the surface of macrophages. In contrast, CpG single-stranded DNA mimics the unmethylated

CpG motifs that are prevalent in bacterial and viral genomes but not vertebrate genomes, and are recognized within endosomes on the interior of the cell. Due to the location of the receptor, the differential recruitment of adaptors by the receptors, and the primary type of pathogen that they recognize, both LPS and CpG elicit dynamics that are specific to their signal: LPS/TLR4 primarily responds to extracellular bacteria, while CpG/TLR9 primarily responds to intracellular bacteria and viruses.

We may hypothesize, then, that the pathogen signals and their respective receptors encode a kinetic profile that is tailored to the specific pathogen challenge at hand. In the case of LPS, the presence of the TLR agonist is indicative of a possible bacterial infection exterior to cell; therefore, a well-suited TNF secretion kinetic profile would likely need to be early, strong, and signal in a predominately paracrine manner. In the case of CpG, engagement of the TLR9 receptor is indicative of a likely bacterial or viral infection within the host cell. Here, the infected cell needs to undergo an appropriate response. Unlike LPS, which leads to the activation of both MyD88 and TRIF pathways leading to prolonged NFκB activation, CpG only leads to the activation of the MyD88 pathway and its strong but transient NFκB activation. As a result, CpG can only bring about persistent NFκB activation by producing TNF and responding to it in an autocrine manner. The fashion in which CpG-induced TNF signals may suggest that the signaling network dynamics downstream of TLR9 are tailored to maximize the response within

the infected host cell without overly propagating the inflammatory signal to neighboring cells that may not be infected. In this aspect, TNF production and autocrine signaling serves as a decision point for the infected cell: as prolonged NFκB activation counteracts programmed cell death, only infected cells that remain healthy enough to produce TNF and respond to it can make the decision to continue to fight the pathogen infection. Cells that can no longer activate these regulatory mechanisms will not be able to produce TNF and therefore may not prolong NFκB activation, allowing for the possibility of stemming the infection via programmed cell death. Although speculative, this hypothesis of regulatory 'design principles' is based on the network dynamics of TNF production and signaling that were revealed by this thesis work. In the inflammatory signaling network, the role of TNF autocrine feedback is analogous in many aspects to that of the TRIF pathway; both lead to persistent NFκB activation and induction of genes involved in propagating the inflammatory signal and macrophage function, albeit by different mechanisms.

Macrophages are known for their pro-inflammatory cytokine production and phagocytotic ability. However, there is a spectrum of functions that macrophages carry out depending on their state, including the attenuation of inflammation and modulation of adaptive immunity. The role that TNF plays in inflammation and innate immunity has been well studied, and in this thesis we show that CpG-induced TNF can signal in autocrine ways, not only affecting proinflammatory cytokine production, but influencing macrophage bacterial

recognition and killing, attenuation of inflammation, and the interaction with adaptive immune cell types. This work highlights the pro-inflammatory role that autocrine TNF plays to prolong NFκB activation as well as the role that it plays in alternative macrophage immune functions.

A goal of the systems biology approach is to develop quantitatively predictive models of regulatory networks. However, the vast and interconnected nature of immune signaling networks present a challenge to developing mechanistic models. In this thesis work, we employed the strategy of 'modular' biology (Hartwell et al., 1999; Kitano, 2002; Mallavarapu et al., 2009b) by focusing our experimental tools to separable regulatory modules and parameterizing corresponding mechanistic, yet simple, coarse-grained ODE-based models. In a modular fashion, we combined the model for TNF production with previously published model for TNFR to IKK activation, TLR to IKK activation, and IKK to NFκB activation to create a mathematical model for TNF signaling within the inflammatory signaling network. This study demonstrates the benefits of the modular approach: the ability to make meaningful predictions. While the TNF production model was trained on LPS perturbation, iterative refinement of the multi-modular model allowed for the prediction of dynamics elicited by alternative TLR agonists CpG and PolyI:C. Furthermore, the model predicted that autocrine TNF signaling would be important for persistent NFκB activity in response to transient stimuli, but not persistent stimuli, which was experimentally validated for CpG and LPS,

respectively. This TNF signaling network model represents a research tool for studies on not only of the dynamics and underlying mechanisms of TNF production, but also of the signaling functions of TNF.

We have constructed a mathematical model for TNF production and signaling within the inflammatory signaling network that is able to recapitulate experimental data for a variety of signal inputs and make useful predictions about the autocrine and paracrine signaling effect of TNF. However, there are important, parrallel pathways within the inflammatory and innate immune signaling network that are interconnected to those described in the TNF signaling network model. In addition to activating NFκB, LPS activates the transcription factor IRF3, which leads to the production of type-1 IFN and innate immune gene programs. With the significant overlap between these gene programs the broadly-inflammatory gene programs controlled by NFκB, a potentially fruitful future direction would be the integration of TNF/NFκB model presented here with a model for the IRF/IFN/STAT module of the innate immune signaling network. This would allow for the construction of a mathematical model that describes the signaling events brought about by the two main cytokines involved in the context of not only TLR-induced signaling, but in inflammation and innate immunity as a whole.

In Chapter 3 of this thesis work, we focused on using the multi-modular model to make predictions about the autocrine and paracrine signaling functions of TNF. However, this model could be used to investigate a number

of other questions as well, including dose-responses, duration of inflammatory signaling within the network, or the spread of an inflammatory signal within a tissue environment. Furthermore, although the network model in its current form is relatively coarse-grained, it can easily serve as a basis for fine-tuning through the encorporation of additional mechanisms. The model was parameterized using specific doses of LPS and CpG that lead initial persistent or transient NFκB activation, respectively. The model could be used to simulate dose-responses for LPS and CpG to determine the initial stimulus signal required to transition from a transient to persistent initial NFκB activation. Further, the model could be simulated to predict the level of initial stimulus required to produce TNF that can sufficiently signal in an autocrine manner to prolong NFκB activity.

This dissertation uses a systems biology approach to experimentally and computationally characterize TNF production in the context of TLR signaling. This modular approach reveals that TNF's autocrine and paracrine functions are stimulus or TLR-specific, determined by the underlying signaling network dynamics of TNF production and NFκB response.

REFERENCES

Aderem, A., and Underhill, D.M. (1999). Mechanisms of phagocytosis in macrophages. Annu. Rev. Immunol. *17*, 593–623.

Aggarwal, B.B., Kohr, W.J., Hass, P.E., Moffat, B., Spencer, S.A., Henzel, W.J., Bringman, T.S., Nedwin, G.E., Goeddel, D.V., and Harkins, R.N. (1985). Human tumor necrosis factor. Production, purification, and characterization. J. Biol. Chem. *260*, 2345–2354.

Akira, S., Hirano, T., Taga, T., and Kishimoto, T. (1990). Biology of multifunctional cytokines: IL 6 and related molecules (IL 1 and TNF). FASEB J. *4*, 2860–2867.

Akira, S., Uematsu, S., and Takeuchi, O. (2006). Pathogen recognition and innate immunity. Cell *124*, 783–801.

Aldridge, B.B., Burke, J.M., Lauffenburger, D.A., and Sorger, P.K. (2006). Physicochemical modelling of cell signalling pathways. Nat. Cell Biol. *8*, 1195–1203.

Alexopoulou, L., Kranidioti, K., Xanthoulea, S., Denis, M., Kotanidou, A., Douni, E., Blackshear, P.J., Kontoyiannis, D.L., and Kollias, G. (2006). Transmembrane TNF protects mutant mice against intracellular bacterial infections, chronic inflammation and autoimmunity. Eur. J. Immunol. *36*, 2768–2780.

Anders, S., Pyl, P.T., and Huber, W. (2014). HTSeq – A Python framework to work with high-throughput sequencing data. bioRxiv.

Andersson, K., and Sundler, R. (2006). Posttranscriptional regulation of TNFalpha expression via eukaryotic initiation factor 4E (eIF4E) phosphorylation in mouse macrophages. Cytokine *33*, 52–57.

Basak, S., Behar, M., and Hoffmann, A. (2012). Lessons from mathematically modeling the NF-κB pathway. Immunol. Rev. *246*, 221–238.

Bethea, J.R., Gillespie, G.Y., and Benveniste, E.N. (1992). Interleukin-1β induction of TNF-α gene expression: Involvement of protein kinase C. J. Cell. Physiol. *152*, 264–273.

Beutler, B., Greenwald, D., Hulmes, J.D., Chang, M., Pan, Y.C., Mathison, J., Ulevitch, R., and Cerami, A. (1985a). Identity of tumour necrosis factor and the macrophage-secreted factor cachectin. Nature *316*, 552–554.

Beutler, B.A., Milsark, I.W., and Cerami, A. (1985b). Cachectin/tumor necrosis factor: production, distribution, and metabolic fate in vivo. J. Immunol. Baltim. Md 1950 *135*, 3972–3977.

Biswas, S.K., and Mantovani, A. (2010). Macrophage plasticity and interaction with lymphocyte subsets: cancer as a paradigm. Nat. Immunol. *11*, 889–896.

Black, R.A., Rauch, C.T., Kozlosky, C.J., Peschon, J.J., Slack, J.L., Wolfson, M.F., Castner, B.J., Stocking, K.L., Reddy, P., Srinivasan, S., et al. (1997). A metalloproteinase disintegrin that releases tumour-necrosis factor-alpha from cells. Nature *385*, 729–733.

Blasi, E., Pitzurra, L., Bartoli, A., Puliti, M., and Bistoni, F. (1994). Tumor necrosis factor as an autocrine and paracrine signal controlling the macrophage secretory response to Candida albicans. Infect. Immun. *62*, 1199–1206.

Carballo, E., Lai, W.S., and Blackshear, P.J. (1998). Feedback inhibition of macrophage tumor necrosis factor-alpha production by tristetraprolin. Science *281*, 1001–1005.

Carswell, E.A., Old, L.J., Kassel, R.L., Green, S., Fiore, N., and Williamson, B. (1975). An endotoxin-induced serum factor that causes necrosis of tumors. Proc. Natl. Acad. Sci. U. S. A. *72*, 3666–3670.

Charo, I.F., and Ransohoff, R.M. (2006). The many roles of chemokines and chemokine receptors in inflammation. N. Engl. J. Med. *354*, 610–621.

Cheng, Z., Taylor, B., Rios, D., and Hoffmann, A. Dynamical characteristics of TLR-responses determined by pathway-specific molecular mechanisms. Under review.

Clark, A., Dean, J., Tudor, C., and Saklatvala, J. (2009). Post-transcriptional gene regulation by MAP kinases via AU-rich elements. Front. Biosci. Landmark Ed. *14*, 847–871.

Covert, M.W., Leung, T.H., Gaston, J.E., and Baltimore, D. (2005). Achieving stability of lipopolysaccharide-induced NF-kappaB activation. Science *309*, 1854–1857.

Coward, W.R., Okayama, Y., Sagara, H., Wilson, S.J., Holgate, S.T., and Church, M.K. (2002). NF-kappa B and TNF-alpha: a positive autocrine loop in human lung mast cells? J. Immunol. Baltim. Md 1950 *169*, 5287–5293.

Damme, J.V., and Mantovani, A. (2005). From cytokines to chemokines. Cytokine Growth Factor Rev. *16*, 549–551.

Datta, S., Novotny, M., Li, X., Tebo, J., and Hamilton, T.A. (2004). Toll IL-1 receptors differ in their ability to promote the stabilization of adenosine and uridine-rich elements containing mRNA. J. Immunol. Baltim. Md 1950 *173*, 2755–2761.

Díaz-Rodríguez, E., Montero, J.C., Esparís-Ogando, A., Yuste, L., and Pandiella, A. (2002). Extracellular signal-regulated kinase phosphorylates tumor necrosis factor alpha-converting enzyme at threonine 735: a potential role in regulated shedding. Mol. Biol. Cell *13*, 2031–2044.

Dobin, A., Davis, C.A., Schlesinger, F., Drenkow, J., Zaleski, C., Jha, S., Batut, P., Chaisson, M., and Gingeras, T.R. (2013). STAR: ultrafast universal RNA-seq aligner. Bioinformatics *29*, 15–21.

Drouet, C., Shakhov, A.N., and Jongeneel, C.V. (1991). Enhancers and transcription factors controlling the inducibility of the tumor necrosis factor-alpha promoter in primary macrophages. J. Immunol. Baltim. Md 1950 *147*, 1694–1700.

Fan, H., and Derynck, R. (1999). Ectodomain shedding of TGF-alpha and other transmembrane proteins is induced by receptor tyrosine kinase activation and MAP kinase signaling cascades. EMBO J. *18*, 6962–6972.

Fan, X.C., and Steitz, J.A. (1998). Overexpression of HuR, a nuclear-cytoplasmic shuttling protein, increases the in vivo stability of ARE-containing mRNAs. EMBO J. *17*, 3448–3460.

Feldman, K.E., Loriaux, P.M., Saito, M., Tuero, I., Villaverde, H., Siva, T., Gotuzzo, E., Gilman, R.H., Hoffmann, A., and Vinetz, J.M. (2013). Ex vivo innate immune cytokine signature of enhanced risk of relapsing brucellosis. PLoS Negl. Trop. Dis. *7*, e2424.

Flicek, P., Amode, M.R., Barrell, D., Beal, K., Brent, S., Carvalho-Silva, D., Clapham, P., Coates, G., Fairley, S., Fitzgerald, S., et al. (2012). Ensembl 2012. Nucleic Acids Res. *40*, D84–D90.

Gais, P., Tiedje, C., Altmayr, F., Gaestel, M., Weighardt, H., and Holzmann, B. (2010). TRIF signaling stimulates translation of TNF-alpha mRNA via prolonged activation of MK2. J. Immunol. Baltim. Md 1950 *184*, 5842–5848.

Gillett, A., Marta, M., Jin, T., Tuncel, J., Leclerc, P., Nohra, R., Lange, S., Holmdahl, R., Olsson, T., Harris, R.A., et al. (2010). TNF production in macrophages is genetically determined and regulates inflammatory disease in rats. J. Immunol. Baltim. Md 1950 *185*, 442–450.

Grivennikov, S.I., Tumanov, A.V., Liepinsh, D.J., Kruglov, A.A., Marakusha, B.I., Shakhov, A.N., Murakami, T., Drutskaya, L.N., Förster, I., Clausen, B.E., et al. (2005). Distinct and nonredundant in vivo functions of TNF produced by t cells and macrophages/neutrophils: protective and deleterious effects. Immunity *22*, 93–104.

Häcker, H., Vabulas, R.M., Takeuchi, O., Hoshino, K., Akira, S., and Wagner, H. (2000). Immune cell activation by bacterial CpG-DNA through myeloid differentiation marker 88 and tumor necrosis factor receptor-associated factor (TRAF)6. J. Exp. Med. *192*, 595–600.

Han, J., Huez, G., and Beutler, B. (1991a). Interactive effects of the tumor necrosis factor promoter and 3'-untranslated regions. J. Immunol. Baltim. Md 1950 *146*, 1843–1848.

Han, J.H., Beutler, B., and Huez, G. (1991b). Complex regulation of tumor necrosis factor mRNA turnover in lipopolysaccharide-activated macrophages. Biochim. Biophys. Acta *1090*, 22–28.

Hao, S., and Baltimore, D. (2009). The stability of mRNA influences the temporal order of the induction of genes encoding inflammatory molecules. Nat. Immunol. *10*, 281–288.

Hartwell, L.H., Hopfield, J.J., Leibler, S., and Murray, A.W. (1999). From molecular to modular cell biology. Nature *402*, C47–52.

Hitti, E., Iakovleva, T., Brook, M., Deppenmeier, S., Gruber, A.D., Radzioch, D., Clark, A.R., Blackshear, P.J., Kotlyarov, A., and Gaestel, M. (2006). Mitogen-activated protein kinase-activated protein kinase 2 regulates tumor necrosis factor mRNA stability and translation mainly by altering tristetraprolin expression, stability, and binding to adenine/uridine-rich element. Mol. Cell. Biol. *26*, 2399–2407.

Hoebe, K., Janssen, E.M., Kim, S.O., Alexopoulou, L., Flavell, R.A., Han, J., and Beutler, B. (2003). Upregulation of costimulatory molecules induced by lipopolysaccharide and double-stranded RNA occurs by Trif-dependent and Trif-independent pathways. Nat. Immunol. *4*, 1223–1229.

Hoebe, K., Janssen, E., and Beutler, B. (2004). The interface between innate and adaptive immunity. Nat. Immunol. *5*, 971–974.

Hoffmann, A., Levchenko, A., Scott, M.L., and Baltimore, D. (2002). The IkappaB-NF-kappaB signaling module: temporal control and selective gene activation. Science *298*, 1241–1245.

Horng, T., Barton, G.M., and Medzhitov, R. (2001). TIRAP: an adapter molecule in the Toll signaling pathway. Nat. Immunol. *2*, 835–841.

Iwasaki, A., and Medzhitov, R. (2010). Regulation of adaptive immunity by the innate immune system. Science *327*, 291–295.

Janes, K.A., Albeck, J.G., Gaudet, S., Sorger, P.K., Lauffenburger, D.A., and Yaffe, M.B. (2005). A systems model of signaling identifies a molecular basis set for cytokine-induced apoptosis. Science *310*, 1646–1653.

Janes, K.A., Gaudet, S., Albeck, J.G., Nielsen, U.B., Lauffenburger, D.A., and Sorger, P.K. (2006). The response of human epithelial cells to TNF involves an inducible autocrine cascade. Cell *124*, 1225–1239.

Johnson, B.A., Stehn, J.R., Yaffe, M.B., and Blackwell, T.K. (2002). Cytoplasmic localization of tristetraprolin involves 14-3-3-dependent and -independent mechanisms. J. Biol. Chem. *277*, 18029–18036.

Kawai, T., and Akira, S. (2006). Innate immune recognition of viral infection. Nat. Immunol. *7*, 131–137.

Kawai, T., and Akira, S. (2010). The role of pattern-recognition receptors in innate immunity: update on Toll-like receptors. Nat. Immunol. *11*, 373–384.

Kawai, T., Adachi, O., Ogawa, T., Takeda, K., and Akira, S. (1999). Unresponsiveness of MyD88-deficient mice to endotoxin. Immunity *11*, 115–122.

Kawakami, M., and Cerami, A. (1981). Studies of endotoxin-induced decrease in lipoprotein lipase activity. J. Exp. Med. *154*, 631–639.

Kearns, J.D., Basak, S., Werner, S.L., Huang, C.S., and Hoffmann, A. (2006). IkappaBepsilon provides negative feedback to control NF-kappaB oscillations, signaling dynamics, and inflammatory gene expression. J. Cell Biol. *173*, 659–664.

Kindler, V., Sappino, A.P., Grau, G.E., Piguet, P.F., and Vassalli, P. (1989). The inducing role of tumor necrosis factor in the development of bactericidal granulomas during BCG infection. Cell *56*, 731–740.

Kitano, H. (2002). Computational systems biology. Nature *420*, 206–210.

Kontoyiannis, D., Pasparakis, M., Pizarro, T.T., Cominelli, F., and Kollias, G. (1999). Impaired on/off regulation of TNF biosynthesis in mice lacking TNF AU-rich elements: implications for joint and gut-associated immunopathologies. Immunity *10*, 387–398.

Kotlyarov, A., Neininger, A., Schubert, C., Eckert, R., Birchmeier, C., Volk, H.D., and Gaestel, M. (1999). MAPKAP kinase 2 is essential for LPS-induced TNF-alpha biosynthesis. Nat. Cell Biol. *1*, 94–97.

Kumar, H., Kawai, T., and Akira, S. (2011). Pathogen recognition by the innate immune system. Int. Rev. Immunol. *30*, 16–34.

Kuno, R., Wang, J., Kawanokuchi, J., Takeuchi, H., Mizuno, T., and Suzumura, A. (2005). Autocrine activation of microglia by tumor necrosis factor-alpha. J. Neuroimmunol. *162*, 89–96.

Lai, W.S., Carballo, E., Strum, J.R., Kennington, E.A., Phillips, R.S., and Blackshear, P.J. (1999). Evidence that tristetraprolin binds to AU-rich elements and promotes the deadenylation and destabilization of tumor necrosis factor alpha mRNA. Mol. Cell. Biol. *19*, 4311–4323.

Lee, T.K., Denny, E.M., Sanghvi, J.C., Gaston, J.E., Maynard, N.D., Hughey, J.J., and Covert, M.W. (2009). A noisy paracrine signal determines the cellular NF-kappaB response to lipopolysaccharide. Sci. Signal. *2*, ra65.

Lombardo, E., Alvarez-Barrientos, A., Maroto, B., Boscá, L., and Knaus, U.G. (2007). TLR4-mediated survival of macrophages is MyD88 dependent and requires TNF-alpha autocrine signalling. J. Immunol. Baltim. Md 1950 *178*, 3731–3739.

Mallavarapu, A., Thomson, M., Ullian, B., and Gunawardena, J. (2009a). Programming with models: modularity and abstraction provide powerful capabilities for systems biology. J. R. Soc. Interface *6*, 257–270.

Mallavarapu, A., Thomson, M., Ullian, B., and Gunawardena, J. (2009b). Programming with models: modularity and abstraction provide powerful capabilities for systems biology. J. R. Soc. Interface R. Soc. *6*, 257–270.

Michlewska, S., Dransfield, I., Megson, I.L., and Rossi, A.G. (2009). Macrophage phagocytosis of apoptotic neutrophils is critically regulated by the opposing actions of pro-inflammatory and anti-inflammatory agents: key role for TNF-alpha. FASEB J. Off. Publ. Fed. Am. Soc. Exp. Biol. *23*, 844–854.

Mosser, D.M., and Edwards, J.P. (2008). Exploring the full spectrum of macrophage activation. Nat. Rev. Immunol. *8*, 958–969.

Murray, P.J., and Wynn, T.A. (2011). Obstacles and opportunities for understanding macrophage polarization. J. Leukoc. Biol. *89*, 557–563.

Nakaya, T., Sato, M., Hata, N., Asagiri, M., Suemori, H., Noguchi, S., Tanaka, N., and Taniguchi, T. (2001). Gene induction pathways mediated by distinct

IRFs during viral infection. Biochem. Biophys. Res. Commun. *283*, 1150–1156.

O'Dea, E., and Hoffmann, A. (2009). NF-κB signaling. Wiley Interdiscip. Rev. Syst. Biol. Med. *1*, 107–115.

O'Dea, E., and Hoffmann, A. (2010). The regulatory logic of the NF-kappaB signaling system. Cold Spring Harb. Perspect. Biol. *2*, a000216.

O'Dea, E.L., Barken, D., Peralta, R.Q., Tran, K.T., Werner, S.L., Kearns, J.D., Levchenko, A., and Hoffmann, A. (2007). A homeostatic model of IkappaB metabolism to control constitutive NF-kappaB activity. Mol. Syst. Biol. *3*, 111.

O'Malley, W.E., Achinstein, B., and Shear, M.J. (1962). Action of Bacterial Polysaccharide on Tumors. II. Damage of Sarcoma 37 by Serum of Mice Treated With Serratia Marcescens Polysaccharide, and Induced Tolerance. J. Natl. Cancer Inst. *29*, 1169–1175.

Osman, F., Jarrous, N., Ben-Asouli, Y., and Kaempfer, R. (1999). A cis-acting element in the 3'-untranslated region of human TNF-alpha mRNA renders splicing dependent on the activation of protein kinase PKR. Genes Dev. *13*, 3280–3293.

Ozaki, Y., Sasagawa, S., and Kuroda, S. (2005). Dynamic characteristics of transient responses. J. Biochem. (Tokyo) *137*, 659–663.

Parameswaran, N., and Patial, S. (2010). Tumor necrosis factor-α signaling in macrophages. Crit. Rev. Eukaryot. Gene Expr. *20*, 87–103.

Peng, S.S., Chen, C.Y., Xu, N., and Shyu, A.B. (1998). RNA stabilization by the AU-rich element binding protein, HuR, an ELAV protein. EMBO J. *17*, 3461–3470.

Pestka, S., Krause, C.D., and Walter, M.R. (2004). Interferons, interferon-like cytokines, and their receptors. Immunol. Rev. *202*, 8–32.

Platanias, L.C. (2005). Mechanisms of type-I- and type-II-interferon-mediated signalling. Nat. Rev. Immunol. *5*, 375–386.

Purvis, J.E., and Lahav, G. (2013). Encoding and Decoding Cellular Information through Signaling Dynamics. Cell *152*, 945–956.

Ronkina, N., Kotlyarov, A., Dittrich-Breiholz, O., Kracht, M., Hitti, E., Milarski, K., Askew, R., Marusic, S., Lin, L.-L., Gaestel, M., et al. (2007). The mitogen-activated protein kinase (MAPK)-activated protein kinases MK2 and MK3

cooperate in stimulation of tumor necrosis factor biosynthesis and stabilization of p38 MAPK. Mol. Cell. Biol. *27*, 170–181.

Salkowski, C.A., Detore, G., McNally, R., van Rooijen, N., and Vogel, S.N. (1997). Regulation of inducible nitric oxide synthase messenger RNA expression and nitric oxide production by lipopolysaccharide in vivo: the roles of macrophages, endogenous IFN-gamma, and TNF receptor-1-mediated signaling. J. Immunol. Baltim. Md 1950 *158*, 905–912.

Sandler, H., and Stoecklin, G. (2008). Control of mRNA decay by phosphorylation of tristetraprolin. Biochem. Soc. Trans. *36*, 491–496.

Sato, S., Sugiyama, M., Yamamoto, M., Watanabe, Y., Kawai, T., Takeda, K., and Akira, S. (2003). Toll/IL-1 receptor domain-containing adaptor inducing IFN-beta (TRIF) associates with TNF receptor-associated factor 6 and TANK-binding kinase 1, and activates two distinct transcription factors, NF-kappa B and IFN-regulatory factor-3, in the Toll-like receptor signaling. J. Immunol. Baltim. Md 1950 *171*, 4304–4310.

Schmittgen, T.D., and Livak, K.J. (2008). Analyzing real-time PCR data by the comparative CT method. Nat. Protoc. *3*, 1101–1108.

Schneider-Brachert, W., Tchikov, V., Neumeyer, J., Jakob, M., Winoto-Morbach, S., Held-Feindt, J., Heinrich, M., Merkel, O., Ehrenschwender, M., Adam, D., et al. (2004). Compartmentalization of TNF Receptor 1 Signaling: Internalized TNF Receptosomes as Death Signaling Vesicles. Immunity *21*, 415–428.

Serbina, N.V., Salazar-Mather, T.P., Biron, C.A., Kuziel, W.A., and Pamer, E.G. (2003). TNF/iNOS-producing dendritic cells mediate innate immune defense against bacterial infection. Immunity *19*, 59–70.

Shih, V.F.-S., Tsui, R., Caldwell, A., and Hoffmann, A. (2011). A single NFκB system for both canonical and non-canonical signaling. Cell Res. *21*, 86–102.

Shirai, T., Yamaguchi, H., Ito, H., Todd, C.W., and Wallace, R.B. (1985). Cloning and expression in Escherichia coli of the gene for human tumour necrosis factor. Nature *313*, 803–806.

Smith, R.A., and Baglioni, C. (1987). The active form of tumor necrosis factor is a trimer. J. Biol. Chem. *262*, 6951–6954.

Soond, S.M., Everson, B., Riches, D.W.H., and Murphy, G. (2005). ERK-mediated phosphorylation of Thr735 in TNFalpha-converting enzyme and its potential role in TACE protein trafficking. J. Cell Sci. *118*, 2371–2380.

Stoecklin, G., Stubbs, T., Kedersha, N., Wax, S., Rigby, W.F.C., Blackwell, T.K., and Anderson, P. (2004). MK2-induced tristetraprolin:14-3-3 complexes prevent stress granule association and ARE-mRNA decay. EMBO J. *23*, 1313–1324.

Striz, I., Brabcova, E., Kolesar, L., and Sekerkova, A. (2014). Cytokine networking of innate immunity cells: a potential target of therapy. Clin. Sci. Lond. Engl. 1979 *126*, 593–612.

Takeuchi, O., and Akira, S. (2010). Pattern recognition receptors and inflammation. Cell *140*, 805–820.

Topisirovic, I., Ruiz-Gutierrez, M., and Borden, K.L.B. (2004). Phosphorylation of the eukaryotic translation initiation factor eIF4E contributes to its transformation and mRNA transport activities. Cancer Res. *64*, 8639–8642.

Wang, A.M., Creasey, A.A., Ladner, M.B., Lin, L.S., Strickler, J., Van Arsdell, J.N., Yamamoto, R., and Mark, D.F. (1985). Molecular cloning of the complementary DNA for human tumor necrosis factor. Science *228*, 149–154.

Wang, L., Trebicka, E., Fu, Y., Waggoner, L., Akira, S., Fitzgerald, K.A., Kagan, J.C., and Cherayil, B.J. (2011). Regulation of lipopolysaccharide-induced translation of tumor necrosis factor-alpha by the toll-like receptor 4 adaptor protein TRAM. J. Innate Immun. *3*, 437–446.

Wang, X., Flynn, A., Waskiewicz, A.J., Webb, B.L., Vries, R.G., Baines, I.A., Cooper, J.A., and Proud, C.G. (1998). The phosphorylation of eukaryotic initiation factor eIF4E in response to phorbol esters, cell stresses, and cytokines is mediated by distinct MAP kinase pathways. J. Biol. Chem. *273*, 9373–9377.

Waters, J.P., Pober, J.S., and Bradley, J.R. (2013). Tumour necrosis factor and cancer. J. Pathol. *230*, 241–248.

Werner, S.L., Barken, D., and Hoffmann, A. (2005). Stimulus specificity of gene expression programs determined by temporal control of IKK activity. Science *309*, 1857–1861.

Werner, S.L., Kearns, J.D., Zadorozhnaya, V., Lynch, C., O'Dea, E., Boldin, M.P., Ma, A., Baltimore, D., and Hoffmann, A. (2008). Encoding NF-kappaB temporal control in response to TNF: distinct roles for the negative regulators IkappaBalpha and A20. Genes Dev. *22*, 2093–2101.

Wesche, H., Henzel, W.J., Shillinglaw, W., Li, S., and Cao, Z. (1997). MyD88: an adapter that recruits IRAK to the IL-1 receptor complex. Immunity *7*, 837–847.

Wu, S., Boyer, C.M., Whitaker, R.S., Berchuck, A., Wiener, J.R., Weinberg, J.B., and Bast, R.C., Jr (1993). Tumor necrosis factor alpha as an autocrine and paracrine growth factor for ovarian cancer: monokine induction of tumor cell proliferation and tumor necrosis factor alpha expression. Cancer Res. *53*, 1939–1944.

Xaus, J., Comalada, M., Valledor, A.F., Lloberas, J., López-Soriano, F., Argilés, J.M., Bogdan, C., and Celada, A. (2000). LPS induces apoptosis in macrophages mostly through the autocrine production of TNF-alpha. Blood *95*, 3823–3831.

Xu, P., and Derynck, R. (2010). Direct activation of TACE-mediated ectodomain shedding by p38 MAP kinase regulates EGF receptor-dependent cell proliferation. Mol. Cell *37*, 551–566.

Yamamoto, M., Sato, S., Hemmi, H., Hoshino, K., Kaisho, T., Sanjo, H., Takeuchi, O., Sugiyama, M., Okabe, M., Takeda, K., et al. (2003). Role of adaptor TRIF in the MyD88-independent toll-like receptor signaling pathway. Science *301*, 640–643.

Zhan, Y., Liu, Z., and Cheers, C. (1996). Tumor necrosis factor alpha and interleukin-12 contribute to resistance to the intracellular bacterium Brucella abortus by different mechanisms. Infect. Immun. *64*, 2782–2786.

Zhao, X.-J., Dong, Q., Bindas, J., Piganelli, J.D., Magill, A., Reiser, J., and Kolls, J.K. (2008). TRIF and IRF-3 binding to the TNF promoter results in macrophage TNF dysregulation and steatosis induced by chronic ethanol. J. Immunol. Baltim. Md 1950 *181*, 3049–3056.